Circuit-QED-based scalable architectures for quantum information processing with superconducting qubits

P.-M. Billangeon,[1,2,*] J. S. Tsai,[1] and Y. Nakamura[2,1]

[1]*RIKEN Center for Emergent Matter Science (CEMS), 2-1 Hirosawa, Wako, Saitama 351-0198, Japan*

[2]*Research Center for Advanced Science and Technology (RCAST), The University of Tokyo, Meguro-ku, Tokyo 153-8904, Japan*

(Received 8 April 2014; revised manuscript received 17 February 2015; published 30 March 2015)

We discuss different ways of generating entanglement in the original picture of circuit QED (XcQED) and several restrictions that arise in the context of a large-scale quantum architecture. To alleviate some of the issues posed by the presence of the nonlinearities inherent to these systems, we introduce a layout for circuit QED, wherein an artificial atom is coupled to a quantized radiation field via its longitudinal degree of freedom (ZcQED). This system is akin to ion traps used in atomic physics, but it relies on fixed coupling between the atom and the resonator. We describe a scalable architecture for processing quantum information with superconducting qubits, which is free from any type of residual interaction between the atomic and photonic degrees of freedom. Tunable interactions can be realized based on sideband transitions, and the system can be operated out of the Lamb-Dicke regime, allowing it to benefit from the possibility of achieving large coupling strengths between atoms and resonators. We also discuss a readout scheme that does not require any extra circuits and allows a *qubit-specific measurement* of the state of the quantum register inspired by the electron shelving technique. This scheme is quantum nondemolition (QND)-like, and allows for single-shot determination of the qubit states.

DOI: 10.1103/PhysRevB.91.094517 PACS number(s): 03.67.Lx, 85.25.Cp, 32.80.Qk

I. INTRODUCTION

The advent of quantum computation relies on the prospect of scaling up the circuits that process information. Solid-state-implemented qubits stand as good candidates to fulfill scalability requirements. Following a proposal by Leggett [1], the first experimental demonstration of macroscopic quantum tunneling of a collective degree of freedom in a current-biased Josephson junction [2] substantiated the possibility of observing macroscopic quantum coherent effects in these systems and thus of building artificial atoms using the nonlinearity provided by the Josephson effect. The first observation of coherent oscillations in a single qubit [3] paved the way for the elaboration of new types of artificial atoms that have a stronger immunity to sources of decoherence [4–7], as well as for generation of entanglement between two or three qubits [8–10], and the demonstration of quantum algorithms [11–13] and quantum error correction [14].

Besides the practical requirements imposed by the necessity of integrating these circuits, the notion of scalability also encompasses various constraints exposed in the seminal work of DiVincenzo [15]: *a scalable physical system with well-characterized qubits*, *the ability to initialize the state of the qubits*, *long decoherence times*, *a "universal" set of quantum gates*, and *a qubit-specific measurement capability*. Decoherence, and more generally errors, remain a major limiting constraint to the manipulation of information encoded in solid-state devices. The field of quantum error correction has striven to tackle this issue with prompt and increasing success since the first code proposed by Shor [16]. The emergence of topological quantum error-correcting codes such as the toric code of Kitaev [17], and subsequently the surface code [18–23], offers a promising solution to these problems. With an error threshold of around 1%, the surface code allows us to envision realistic architectures for processing quantum information to the detriment of a large overhead. Motivated by this approach to quantum error correction, we will consider in this work how to devise a scalable architecture that fulfills the DiVincenzo criteria, and is based on a two-dimensional (2D) array of qubits on a square lattice with tunable nearest-neighbor interactions.

Besides elucidating intricate aspects of field-matter interactions in the quantum regime, the field of atomic physics has been pioneering the realization of different milestones demonstrating how to harness quantum coherence and entanglement for quantum information processing purposes. Cavity quantum electrodynamics, on one hand, has investigated the interaction of a two-level atom with the quantized electromagnetic field of a high-quality-factor cavity at optical or microwave frequencies via the atom's transition dipole moment [24,25]. Experimental implementations include the generation of EPR pairs [26], the demonstration of a quantum phase gate [27] and the realization of a quantum memory [28]. Trapped atomic ions, on the other hand, bring into play charged atoms confined by electromagnetic fields. Trapping allows atomic states to be sustained with relatively long lifetimes by dint of isolation from the environment [29]. Experimental demonstrations comprise the generation of entanglement between up to 14 ions [30–32], the implementation of the Deutsch-Jozsa algorithm [33], the realization of a Toffoli gate [34], and quantum error correction [35,36]. Cirac and Zoller first proposed a scalable system built on a chain of ions in a linear trap [37]. Tunable interactions could be achieved by means of sideband transitions associated with the quantized center-of-mass motion of the ions in the trap [38,39]. Other proposals broached the issue of integration by planarizing the trap [40,41].

The field of circuit QED addresses methods to reproduce and deepen the understanding of coherent interactions between light and matter with superconducting electrical

*To whom all correspondence should be addressed: pierre.billangeon@gmail.com

TABLE I. Comparison between the two architectures presented in this work.

	XcQED	ZcQED
Static coupling	Qubits transversely coupled to four distinct resonators	Qubits longitudinally coupled to four distinct pairs of resonators
Parity symmetry	Yes	No
Residual interactions	Qubit-resonator: dispersive shift (second order), qubit-qubit: residual $\sigma_z\sigma_z$ interactions (fourth order)	No residual interactions
Tunable coupling	via sideband transitions or two-qubit parametric conversion	via sideband transitions: controlled-phase gate *a la* Cirac & Zoller
Readout	via dispersive shift (dispersive readout)	via a combination of two-mode sideband transitions (electron shelving-like)
Purcell effect	Yes	No

circuits [42,43]. Artificial atoms made of Josephson junctions provide coherent two-level systems, whereas quantum harmonic oscillators can be made of either lumped element resonators (single-mode) or coplanar waveguide resonators (multimode). This type of layout offers great versatility for engineering interactions between atomic and photonic degrees of freedom at one's discretion; one of its main advantages is the possibility of reaching the strong coupling regime, i.e., a configuration wherein the coupling strength g between the artificial atom and the microwave photons exceeds the resonator decay rate κ. The aim of the present work is to explore another possibility offered by these systems, which is to couple to these artificial atoms by means of different degrees of freedom, either transverse or longitudinal.

In Sec. II, we will review some basic aspects of the usual picture of circuit QED based on the transverse interaction with the atom, which we will refer to as XcQED. This scheme is an exact analog of cavity QED experiments with solid-state devices. We will present two different ways to realize two-qubit gates via a resonant microwave drive that will allow us to overcome the parity selection rule, and we will discuss various implications of the presence of residual interactions and the justification of the rotating wave approximation (RWA); the latter two constraints set a lower and an upper bound, respectively, on the amplitude of each microwave drive applied to manipulate the state of the quantum register. We will broach the practical consequences of these restrictions on the control of a large-scale system relying on these tunable resonant interactions, and the emergence of correlated errors that must be taken into account in the error model so as to ensure its fault-tolerant operation.

Section III introduces a new paradigm for circuit QED, wherein a qubit is coupled longitudinally to a quantum harmonic oscillator, which we will call ZcQED. We will see that this configuration bears a close resemblance to ion-trap systems, even though the fixed qubit-resonator interaction results in some significant differences such as the existence of residual interactions, which are unlike the purely tunable interactions for trapped ions. This approach is quite favorable for developing a scalable architecture for quantum information processing. Indeed, since the interaction term commutes with the free Hamiltonian of the qubits, once one finds a way to cancel out these parasitic terms at the level of one unit cell coupling two neighboring qubits, this compensation will remain valid inside a 2D array. We will devise a quantum architecture wherein each pair of nearest-neighbors is longitudinally coupled to two resonators that are themselves fixedly coupled via orthogonal degrees of freedom. This configuration guarantees the exact cancellation of all residual interactions between atomic and photonic degrees of freedom, thus providing a quantum register with well-defined energy levels.

We will introduce a means of generating entanglement between each pair of nearest-neighbors via a mechanism of conditional accumulation of global phase inspired by the Cirac-Zoller gate [37], which involves two-mode states of the two resonators mediating the interaction between them. The encoding of the state of one of the two qubits into a two-mode state and its manipulation via two-mode sideband transitions prevent the risk of leakage out of the computational subspace inherent to sideband transitions, without requiring a reduction in the anharmonicity of the artificial atoms. Given that the absence of dispersive shift precludes the determination of the state of each qubit via dispersive readout, we will present an alternative based on the electron shelving technique, which bootstraps the two resonators between each pair of nearest-neighboring qubits and takes advantage of the absence of nonlinearity in the energy spectrum of the system. The analogy with trapped ions is essential in the sense that it enables us to benefit from the theoretical tools already developed in this field. From a practical point of view, mediating the interaction between qubits with microwave resonators made of electrical circuits allows us to move them farther apart from each other: such a configuration facilitates the introduction of control lines and should reduce the risks of cross-talk. A summary of the peculiarities of each scheme is presented in Table I.

The ideas expounded in this manuscript are very generic, but we wish to exemplify their implementation with Josephson qubits. The artificial atom we are considering to use is referred to as a *three-junction flux qubit* [4,44], a variation of the better known *rf-SQUID*, wherein the self-inductance of the loop is replaced by two large Josephson junctions. The main advantage of this device is that it can serve as a good effective two-level system, which can be fairly represented by the Lie group SU(2): therefore effective models based on a representation with Pauli matrices provide an appropriate description of coupled systems, and the risk of leakage of information out of the computational subspace due to excitation of higher energy levels while performing single-qubit and two-qubit operations by microwave irradiation can be safely ignored.

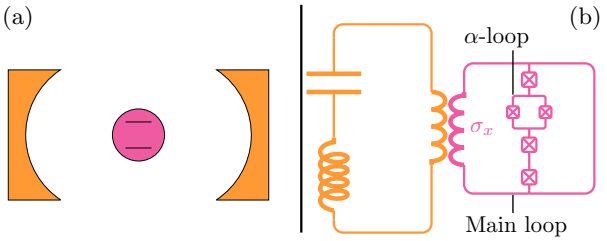

FIG. 1. (Color online) (a) Schematic representation of a cavity QED experiment: a real atom interacts via its electric dipole moment with the electric field of the quantized radiation field of a 3D cavity. (b) Possible implementation of a XcQED experiment with a flux qubit: the artificial atom is transversely coupled to the resonator by inductive coupling to the main loop of the qubit. In this configuration, the qubit can be driven longitudinally (i.e., along σ_z) by modulating the flux through the α-loop (split junction) with a microwave drive.

Another valuable asset is the possibility of separating the longitudinal and transverse degrees of freedom (i.e., σ_z and σ_x, respectively), both for control and coupling of these circuits (see Appendix A). These systems exhibit a rather high sensitivity to fluctuations in their environment. A way to reduce the impact of these external sources of noise is to operate them at the so-called optimal point, i.e., when the magnetic frustration $f = 1/2$ [where $f = \Phi/\Phi_0$, with Φ being the magnetic flux piercing the qubit loop and $\Phi_0 = h/(2e)$ being the superconducting flux quantum]. Subsequently, we will consider solely configurations wherein qubits are biased at the optimal point: it will appear that maintaining this symmetry is essential for exactly compensating for various kinds of residual interactions, which is the crux of this work.

II. TRANSVERSE COUPLING BETWEEN QUBIT AND RESONATOR (XcQED)

Cavity QED addresses systems in atomic physics wherein a real atom is coupled to the quantized electromagnetic field of a high-quality-factor 3D cavity via its electric dipole moment [see Fig. 1(a)]: this type of experimental layout is equivalent to a spin 1/2 that interacts transversely with a single bosonic mode, and is referred to as XcQED. Circuit QED investigates this type of interaction using solid-state devices. Wallraff *et al.* demonstrated the coherent coupling of a superconducting charge qubit transversely coupled to an on-chip microwave resonator in the strong coupling regime [43]. A similar light-matter interaction signature was observed between another artificial atom (transmon) and a 3D cavity by Paik *et al.* [45].

A. Single-qubit case

1. Static Hamiltonian

The Jaynes-Cummings Hamiltonian [46] describes the transverse interaction between a two-level atom and a quantum harmonic oscillator, ignoring the nonsecular term in the interaction:

$$\mathcal{H}_{\rm JC} = \omega_r\, a^\dagger a + \frac{\Delta}{2}\,\sigma_z + g(a^\dagger\sigma_- + a\sigma_+), \tag{1}$$

where $a^\dagger$ and a are bosonic creation and annihilation operators, respectively, and σ_+ and σ_- are atomic raising and lowering operators, respectively. The Jaynes-Cummings Hamiltonian has a continuous U(1) symmetry, as the number of excitations is conserved ($[\mathcal{H}_{\rm JC},\mathcal{N}] = 0$ where $\mathcal{N} = (a^\dagger a + \sigma_+\sigma_-)$ is the total number of excitations). In the dispersive regime ($g/|\Delta - \omega_r| \ll 1$), the static interaction between the atom and the resonator can be fairly well diagonalized by the unitary transformation

$$\mathcal{U} = \exp[\gamma(a^\dagger\sigma_- - a\sigma_+)], \tag{2}$$

where $\gamma = g/(\Delta - \omega_r)$. Expanding the Baker-Campbell-Hausdorff (BCH) formula up to second order, it comes

$$\mathcal{H}'_{\rm JC} = \left(\omega_r + \frac{g^2}{\Delta - \omega_r}\,\sigma_z\right) a^\dagger a + \frac{1}{2}\left(\Delta + \frac{g^2}{\Delta - \omega_r}\right)\sigma_z. \tag{3}$$

At this point, two remarks can be made: we observe a renormalization of the resonant frequency of the atom as $g^2/2(\Delta - \omega_r)$ (Lamb shift), together with a residual interaction between the atomic and photonic longitudinal degrees of freedom as $g^2/(\Delta - \omega_r)$ (Stark shift). This latter component, the so-called dispersive shift, has been extensively used in XcQED to read out the states of qubits using homodyne detection (dispersive readout [47]). A less desirable consequence of this same term is that it makes the qubit relaxation time dependent on the photon lifetime in the resonator (Purcell effect [48,49]), as a consequence of the mixing between the atom and photon states.

Taking into account the nonsecular term in the atom-resonator interaction, we obtain the original Rabi Hamiltonian [50]:

$$\mathcal{H}_{\rm Rabi} = \omega_r\, a^\dagger a + \frac{\Delta}{2}\,\sigma_z + g\,\sigma_x(a^\dagger + a). \tag{4}$$

The Rabi Hamiltonian has a discrete $\mathbb{Z}_2$ symmetry (parity symmetry: $[\mathcal{H}_{\rm Rabi},\Pi] = 0$ where $\Pi = -\sigma_z\, e^{i\pi a^\dagger a}$ is the parity operator), and it is both integrable and exactly solvable as proven by Braak [51]. Zueco *et al.* showed how to simultaneously diagonalize the secular and nonsecular terms in the static interaction, starting from the dispersive unitary transformation introduced earlier in the context of the Jaynes-Cummings Hamiltonian [52]. They introduced the following unitary transformation:

$$\mathcal{U} = \exp[\gamma(a^\dagger\sigma_- - a\sigma_+) - \bar\gamma(a^\dagger\sigma_+ - a\sigma_-)], \tag{5}$$

where $\gamma = g/(\Delta - \omega_r)$ and $\bar\gamma = g/(\Delta + \omega_r)$. Expanding again the BCH formula up to second order, it is found that

$$\mathcal{H}'_{\rm Rabi} = \omega_r\, a^\dagger a + \frac{\Delta}{2}\,\sigma_z + \frac{g^2}{2}\left(\frac{1}{\Delta - \omega_r} + \frac{1}{\Delta + \omega_r}\right)\sigma_z(a^\dagger + a)^2. \tag{6}$$

Analogously to the case of the Jaynes-Cummings Hamiltonian, the resonant frequency of the atom is renormalized by the interaction with the resonator. The dispersive shift now includes two contributions: the Stark shift coming from the secular term $[g^2/(\Delta - \omega_r)]$, and the Bloch-Siegert shift originating from the nonsecular term $[g^2/(\Delta + \omega_r)]$.

2. *Sideband transitions*

The generation of entanglement through sideband transitions was originally introduced in the context of quantum computation with trapped ions [37], and then later extended to the case of XcQED [53]: however, the implementation of sideband transitions in each system is substantially different, as will be shown hereafter. Considering that sideband transitions couple states of same parity, these processes are forbidden when a qubit under a one-photon transverse drive is biased at its symmetry point, as σ_x is an odd parity operator (that is, $\{\Pi,\sigma_x\}=0$, where $\{.,.\}$ denotes an anticommutator). This selection rule can be overcome either by biasing the qubit slightly away from its symmetry point (making the system more sensitive to low-frequency noise thus enhancing dephasing), or by using a two-photon drive (which requires greater amount of microwave power, therefore posing cross-talk issues) [54–56]. Another alternative is to drive the qubit longitudinally [see Fig. 1(b)]: as σ_z is an even parity operator ($[\Pi,\sigma_z]=0$, where $[.,.]$ denotes a commutator), this allows the circumvention of the aforementioned selection rule without affecting the decoherence rate of the atom or the control fidelity of its neighbors. The Hamiltonian of the qubit under a longitudinal microwave drive is given by

$$\mathcal{H}(t)=\mathcal{H}_{\text{Rabi}}+\Omega(t)\cos(\omega t+\phi)\sigma_z, \tag{7}$$

where Ω, ω, and ϕ are the amplitude, the frequency, and the phase of the microwave drive, respectively.

Applying the aforementioned unitary transformation, which diagonalizes the Rabi Hamiltonian, and switching to the rotating frame of the qubit and the resonator with the following time-dependent unitary transformation:

$$\mathcal{U}=\exp\left[-\mathrm{i}\,\frac{(\Delta' t+\phi_q)}{2}\,\sigma_z-\mathrm{i}(\omega_r t+\phi_r)a^\dagger a\right], \tag{8}$$

we obtain the effective Hamiltonian within the RWA:

$$\begin{aligned}
\mathcal{H}^{\text{RWA}}_{\text{red}} &= g(\gamma+\bar{\gamma})\sigma_z\, a^\dagger a-\frac{\Omega(t)}{2}\,2\gamma[\mathrm{e}^{\mathrm{i}\,((\phi_r-\phi_q)-\varsigma\phi)}\,a^\dagger\sigma_-+\mathrm{e}^{-\mathrm{i}((\phi_r-\phi_q)-\varsigma\phi)}a\sigma_+] \quad \text{if} \quad \omega=|\omega_r-\Delta'|/\hbar,\\
\mathcal{H}^{\text{RWA}}_{\text{blue}} &= g(\gamma+\bar{\gamma})\sigma_z\, a^\dagger a-\frac{\Omega(t)}{2}\,2\bar{\gamma}[\mathrm{e}^{\mathrm{i}((\phi_r+\phi_q)-\phi)}a^\dagger\sigma_++\mathrm{e}^{-\mathrm{i}((\phi_r+\phi_q)-\phi)}a\sigma_-] \quad \text{if} \quad \omega=(\omega_r+\Delta')/\hbar,
\end{aligned} \tag{9}$$

where $\Delta'=(\Delta+g(\gamma+\bar{\gamma})/2)$ is the qubit resonant frequency (including the Lamb shift), ϕ_q and ϕ_r are the reference phases of the rotating frame of the qubit and the resonator, respectively, and $\varsigma=\text{sign}(\omega_r-\Delta')$. We confirm the relevance of the above analytic expressions for the matrix elements associated with sideband transitions by comparing them with the result obtained by a numerical diagonalization [see Fig. 2]. Some deviation from the above treatment based on a perturbative expansion can be seen when the dispersive approximation breaks down. The matrix elements corresponding to red sideband transitions do not depend on the sign of the detuning between the qubit and the resonator as one would expect for a process which conserves the number of excitations [see Fig. 2(c)], whereas, in the case of blue sideband transitions, they are given by a monotically decreasing function of the qubit resonant frequency Δ in the dispersive regime [see Fig. 2(d)]. Beaudoin *et al.* discussed a similar layout in a more thorough way, as they took into account the anharmonicity of the device (transmon) [57]. Strand *et al.* demonstrated this idea based on a flux-driven transmon [58].

One disadvantage of this approach is that it renders two-qubit operations based on sideband transitions sensitive to the photon lifetime in the resonator, as it relies on real excitations of the bosonic mode. Two other related issues arise from the dispersive shift. First, considering the typical values of the qubit-resonator coupling strength ($g/h\sim$ few 100 MHz) and detuning ($|\delta|/h=|\Delta-\omega_r|/h\sim$ few GHz) in current XcQED experiments, the dispersive shift is of the order of few tens of MHz, which is not negligible. Considering the achievable speed for this type of microwave-induced interaction, this means that the ON/OFF ratio can be rather low, where the ON/OFF ratio is defined as the quotient of the tunable two-qubit interaction over the residual interaction (viz., the dispersive shift). Second, since sideband transitions bring about real excitations in the resonator, the dispersive shift causes some spurious phase accumulation for the other qubits coupled to it, depending on their state during the idle time between the various sideband transitions. These two effects unavoidably entangle the resonator with the qubits coupled to it, thus generating some leakage of information out of the computational subspace. Consequently, given the somewhat large residual interactions between the atomic and photonic degrees of freedom in XcQED, entanglement generation via sideband transitions suffers from rather severe constraints: an approach that does not involve any real excitation of the resonator would allow us to circumvent the aforesaid issues.

3. *Qubit relaxation*

We denote by γ_{q} the relaxation rate of the qubit due to intrinsic decay processes of the bare qubit state. The eigenstates of the coupled qubit-resonator system $|\overline{n,\psi}\rangle$ are related to the bare states $|n,\psi\rangle$ via

$$|\overline{n,\psi}\rangle=\mathcal{U}|n,\psi\rangle, \tag{10}$$

where $|n\rangle$ corresponds to a Fock state of the resonator, $|\psi\rangle$ is an arbitrary qubit state, and $\mathcal{U}$ is the unitary transformation which diagonalizes the Rabi Hamiltonian [see Eq. (5)]. After expanding the BCH formula up to first order, we arrive at an expression for the lowering operator σ_- in the eigenbasis:

$$\mathcal{U}^\dagger\sigma_-\,\mathcal{U}=\sigma_-+(\gamma\, a\sigma_z+\bar{\gamma}\, a^\dagger\sigma_z). \tag{11}$$

This analysis reveals that the combination of single-qubit relaxation and transverse interactions between atomic and photonic degrees of freedom introduces correlated photon-flip and qubit phase-flip errors. This process is allowed by the parity selection rule. The error rate corresponding to these

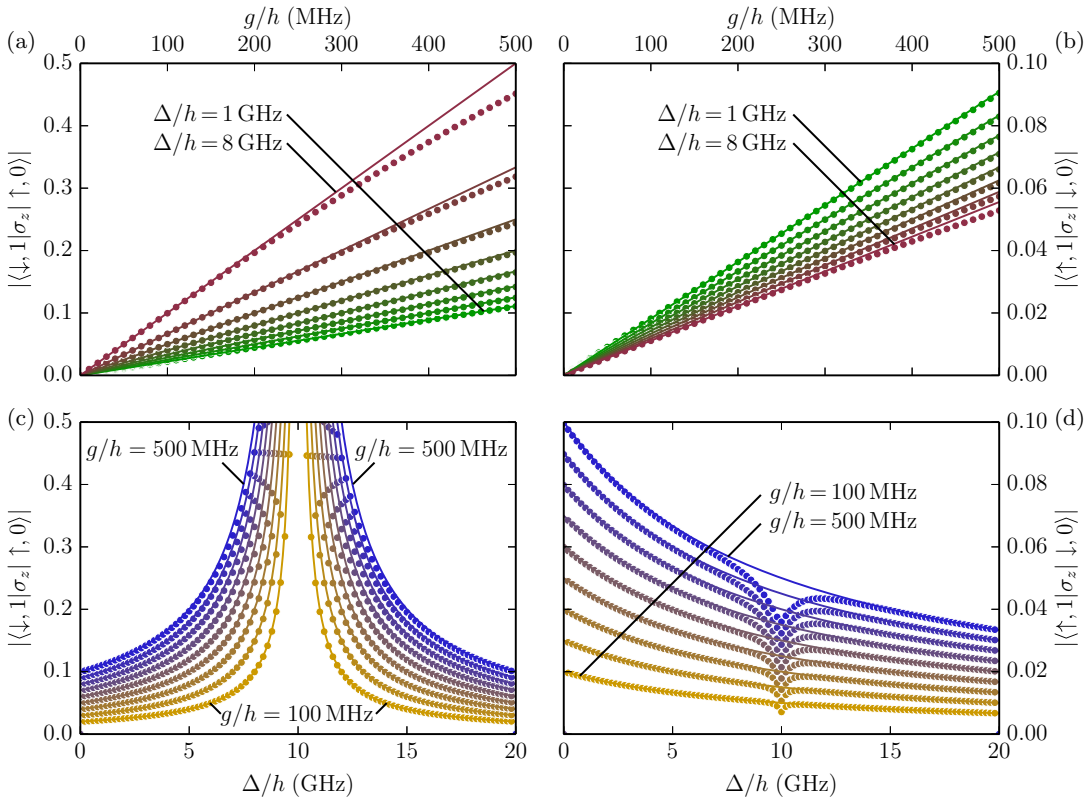

FIG. 2. (Color online) Matrix elements for sideband transitions (red sideband [(a) and (c)] and blue sideband [(b) and (d)]) for a single qubit transversely coupled to a resonator (XcQED - Rabi Hamiltonian) vs the coupling g for different values of $\Delta(\omega_r/h = 10$ GHz and Δ/h ranges from 1 to 8 GHz in steps of 1 GHz) in (a) and (b), and vs the gap Δ for different values of $g(\omega_r/h = 10$ GHz and g/h ranges from 100 to 500 MHz in steps of 50 MHz) in (c) and (d): results obtained by numerical diagonalization of the Rabi Hamiltonian (dots) are compared with perturbative expansion (lines). For numerical diagonalizations, the resonator Hilbert space is truncated to $n = 80$ Fock states.

correlated errors is given by the following:

$$\begin{aligned}\Gamma_{\gamma_q} &= \gamma_q |\langle \overline{0,\mp}|\sigma_-|\overline{1,\pm}\rangle|^2 \\ &= \gamma_q |\langle 0,\mp|\mathcal{U}^\dagger \sigma_- \mathcal{U}|1,\pm\rangle|^2.\end{aligned} \tag{12}$$

where $|\pm\rangle = (|0\rangle \pm |1\rangle)/\sqrt{2}$. Given the expression of the qubit lowering operator in its rotated form, we find that the rate corresponding to these correlated errors reads as follows:

$$\Gamma_{\gamma_q} = \gamma_q \gamma^2. \tag{13}$$

In the context of entanglement generation between two qubits based on sideband transitions, this type of correlated error must be properly taken into account in the procedure for quantum error correction. The dispersive regime is quite favorable in the sense that it allows us to neglect the adverse effects of correlated errors, which arise at higher-order in the expansion of the BCH formula (see Ref. [59]).

B. Two-qubit case

Blais *et al.* thoroughly examined various possibilities for inducing two-qubit interactions in the context of XcQED [53]. Sillanpää *et al.* demonstrated the coherent transfer of quantum states between two phase qubits coupled via a $\lambda/2$ coplanar waveguide resonator by sequentially bringing the qubits and the resonator into resonance with dc pulses [60]. Majer *et al.* simultaneously realized a similar experiment with two transmons: the two-qubit interaction was turned on by tuning both qubits into resonance with an off-resonant microwave pulse (ac-Stark effect) [61]. DiCarlo *et al.* implemented a controlled-phase gate [11] by adiabatically bringing the system close to an avoided crossing with a state outside of the computational subspace, similar to the proposal of Strauch *et al.* [62]. Later, DiCarlo *et al.* extended this mechanism of conditional phase accumulation based on level repulsion to nonadiabatic control [9]. The latter protocols are well suited for artificial atoms with a relatively weak anharmonicity, and do not apply to flux qubits.

Chow *et al.* extended the idea of cross-resonance introduced by Rigetti and Devoret [63] to circuit QED systems [64]. Chow *et al.* demonstrated a microwave-induced controlled-phase gate that relied on an avoided crossing with a state outside of the computational subspace [65]. Even though it is significantly slower than its dc pulsed counterparts, this type of two-qubit gate may be more feasibly scaled up. Poletto *et al.* demonstrated the entanglement of two superconducting qubits in a 3D cavity via a two-photon driving of the $|00\rangle \leftrightarrow |11\rangle$ transition, which is enabled by the anharmonicity of these artificial atoms [66].

Few possible XcQED based architectures have been suggested. Helmer *et al.* described a layout wherein physical qubits are arranged on a 2D square lattice and all qubits sitting either on the same line or in the same column are coupled via the same cavity [67]. Galiautdinov *et al.* introduced an architecture that not only included physical qubits and

resonators to mediate the interaction between them but also quantum memories (RezQu) [68,69]. Earlier, Mariantoni *et al.* reported the operation of a building block of such a system [70].

1. Static Hamiltonian

Let us now consider the case of two qubits transversely coupled to a resonator. Neglecting the nonsecular terms in the static interaction between the qubits and the resonator, the Hamiltonian describing this system reads

$$\mathcal{H}_{\rm JC} = \omega_r\, a^\dagger a + \sum_{i=1,2} \frac{\Delta_i}{2}\,\sigma_i^z + \sum_{i=1,2} g_i(a^\dagger \sigma_i^- + a\sigma_i^+). \quad (14)$$

This Jaynes-Cummings Hamiltonian can be diagonalized using a unitary transformation similar to the one introduced for the single qubit case:

$$\mathcal{U} = \exp\left[\sum_{i=1,2} \gamma_i(a^\dagger\sigma_i^- - a\sigma_i^+)\right], \quad (15)$$

where $\gamma_i = g_i/(\Delta_i - \omega_r)$. By expansion of the BCH formula up to second order, the Hamiltonian for two qubits is given by

$$\begin{aligned}\mathcal{H}'_{\rm JC} = &\left(\omega_r + \sum_{i=1,2} g_i\,\gamma_i\,\sigma_i^z\right) a^\dagger a + \sum_{i=1,2} \frac{(\Delta_i + g_i\,\gamma_i)}{2}\,\sigma_i^z \\ &+ \frac{1}{2}(g_1\,\gamma_2 + g_2\,\gamma_1)(\sigma_1^+\sigma_2^- + \sigma_1^-\sigma_2^+) \\ &+ J_{\rm res}\,\sigma_1^z\sigma_2^z(2\,a^\dagger a + \mathbb{1}), \end{aligned} \quad (16)$$

where $J_{\rm res}$ is the residual $\sigma_z\sigma_z$ interaction between both qubits, which arises at fourth order in the expansion of the BCH formula (see Sec. II B 3). In this new basis, the Hamiltonian contains an effective isotropic XY interaction between both qubits mediated at second order by the resonator, the so-called *flip-flop* interaction [53]. The absence of the nonsecular term in the static two-qubit interaction is a consequence of dropping the nonsecular terms in the initial qubit-resonator interaction.

In a similar manner to what has been shown previously for the single-qubit case, one can account for the nonsecular term in the qubit-resonator fixed interaction in the two-qubit case as well. The Hamiltonian thus reads

$$\mathcal{H}_{\rm Rabi} = \omega_r\, a^\dagger a + \sum_{i=1,2} \frac{\Delta_i}{2}\,\sigma_i^z + \sum_{i=1,2} g_i\,\sigma_i^x(a^\dagger + a). \quad (17)$$

Following again Zueco *et al.* [52], the static interaction between both of the qubits and the resonator can be diagonalized using the unitary transformation as follows:

$$\mathcal{U}_1 = \exp\left\{\sum_{i=1,2}[\gamma_i(a^\dagger\sigma_i^- - a\sigma_i^+) - \bar\gamma_i(a^\dagger\sigma_i^+ - a\sigma_i^-)]\right\}. \quad (18)$$

Based on the expansion of the BCH formula up to fourth order and further diagonalization of the two-photon terms (see Ref. [59] for details of the derivation), Eq. (17) becomes

$$\begin{aligned}\mathcal{H}'_{\rm Rabi} = &\,\omega_r\, a^\dagger a + \sum_{i=1,2} \frac{\Delta'_i}{2}\,\sigma_i^z + \sum_{i=1,2} g_i(\gamma_i + \bar\gamma_i)\sigma_i^z\, a^\dagger a \\ &+ \frac{J_{12}^{xx}}{2}\,\sigma_1^x\sigma_2^x + J_{\rm res}\,\sigma_1^z\sigma_2^z(2\,a^\dagger a + \mathbb{1}), \end{aligned} \quad (19)$$

where $\Delta'_i = (\Delta_i + g_i(\gamma_i + \bar\gamma_i)/2)$ corresponds to each qubit resonant frequency (including the Lamb shift), $J_{12}^{xx} = [g_1(\gamma_2 - \bar\gamma_2) + g_2(\gamma_1 - \bar\gamma_1)]$ is the transverse interaction mediated by the resonator, and $J_{\rm res}$ is the residual $\sigma_z\sigma_z$ interaction between both qubits (see Sec. II B 3). This time, the resonator-mediated interaction between the qubits is of the Ising type, i.e., it includes the nonsecular term $(\sigma_1^+\sigma_2^+ + \sigma_1^-\sigma_2^-)$: the presence of this latter term allows to recover matrix elements for the parametric conversion process from state $|{\downarrow\downarrow}\rangle$ to state $|{\uparrow\uparrow}\rangle$. This transverse interaction mediated by the resonator can be diagonalized in the two-qubit subspace. The secular term can be canceled by applying the unitary transformation:

$$\mathcal{U}_2 = \exp[\theta_1(\sigma_1^+\sigma_2^- - \sigma_1^-\sigma_2^+)], \quad (20)$$

where $\tan(2\theta_1) = J_{12}^{xx}/(\Delta'_1 - \Delta'_2)$. The nonsecular term can be diagonalized with the following unitary transformation:

$$\mathcal{U}_3 = \exp[\theta_2(\sigma_1^+\sigma_2^+ - \sigma_1^-\sigma_2^-)], \quad (21)$$

where $\tan(2\theta_2) = J_{12}^{xx}/(\Delta'_1 + \Delta'_2)$. Eventually, we obtain the Hamiltonian

$$\begin{aligned}\mathcal{H}''_{\rm Rabi} = &\,\omega_r\, a^\dagger a + \frac{\varsigma\,\hbar\omega_-}{4}(\sigma_1^z - \sigma_2^z) + \frac{\hbar\omega_+}{4}(\sigma_1^z + \sigma_2^z) \\ &+ \sum_{i=1,2} g_i(\gamma_i + \bar\gamma_i)\sigma_i^z\, a^\dagger a \\ &+ J_{\rm res}\,\sigma_1^z\sigma_2^z(2\,a^\dagger a + \mathbb{1}), \end{aligned} \quad (22)$$

where $\hbar\omega_\pm = \sqrt{(\Delta'_1 \pm \Delta'_2)^2 + (J_{12}^{xx})^2}$ are the sum and difference of the resonant frequencies of the qubits renormalized by the transverse interaction, and $\varsigma = \mathrm{sign}(\Delta'_1 - \Delta'_2)$.

2. Parametrically induced interactions

Bertet *et al.* discussed the possibility of realizing parametric conversion between the states of two qubits coupled via a resonator [71]. They considered a configuration wherein both qubits are biased at their optimal points, and the resonator is driven at the sum or difference of their frequencies ($\omega = \omega_\pm$). Their conclusion was that parametric conversion between two-qubit states cannot be realized by driving the resonator: similarly to what we described in the case of sideband transitions, this selection rule arises from the fact that parity is conserved in the process of parametric conversion between two-qubit states while the charge q_r and flux ϕ_r of the resonator are odd parity operators. Bertet *et al.* remedied this problem by introducing a nonlinearity into the subcircuit mediating the interaction, which allowed them to circumvent the selection rule by modulating the resonator frequency. Niskanen *et al.* introduced an alternative approach using a qubit as a coupler that was driven transversely at the sum or difference of the frequencies [72]. σ_x also being an odd parity operator, the coupler had to be biased away from its symmetry point. However, in XcQED, even though transversely driving the resonator or one of the qubits does not allow to induce parametric conversion between two-qubit states, an alternative is to longitudinally drive one of the qubits so as to overcome the parity selection rule. Let us assume that we apply a longitudinal microwave drive to the first qubit; the time-dependent Hamiltonian is thus given by

$$\mathcal{H}(t) = \mathcal{H}_{\rm Rabi} + \Omega(t)\cos(\omega t + \phi)\sigma_1^z, \quad (23)$$

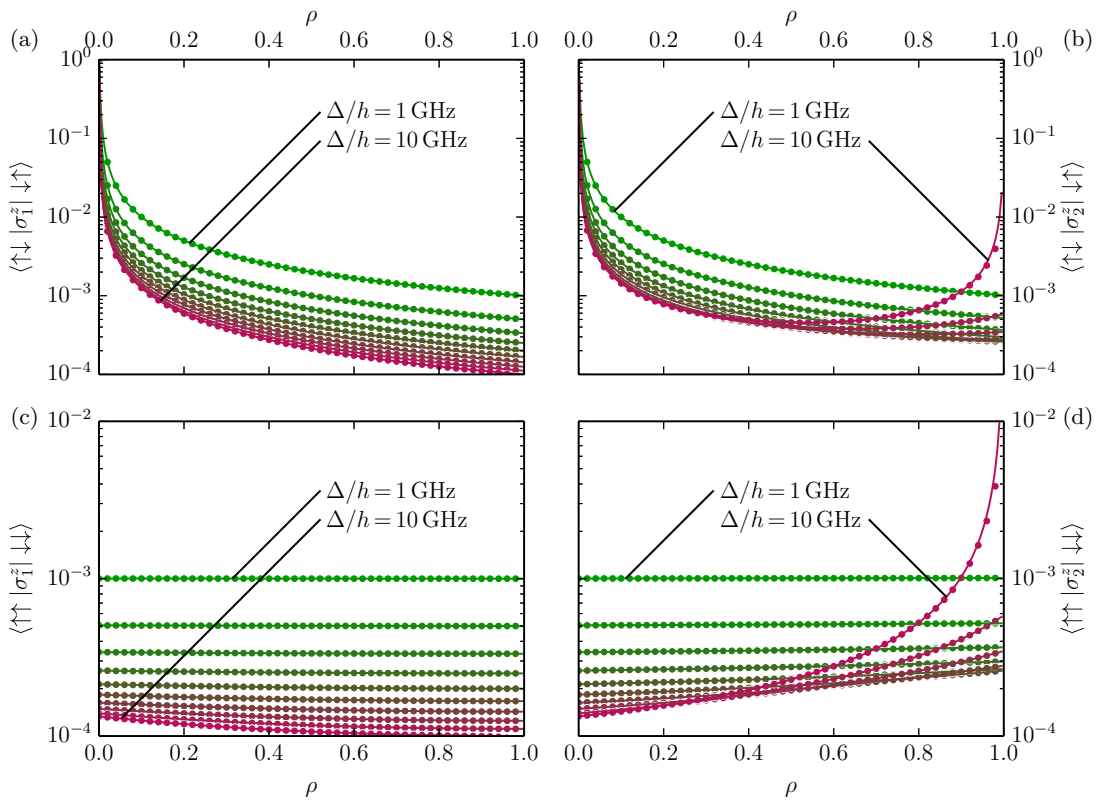

FIG. 3. (Color online) Matrix elements of the parametrically induced iSWAP gate between two qubits coupled to a common resonator (XcQED - Rabi Hamiltonian) vs the asymmetry ρ between their gap [$\Delta_1 = \Delta(1+\rho)$, $\Delta_2 = \Delta(1-\rho)$], for different values of $\Delta(\omega_r/h = 20\ \text{GHz}, g_1/h = g_2/h = 100\ \text{MHz}$, and Δ/h ranges from 1 to 10 GHz in steps of 1 GHz): results obtained from numerical diagonalization of the Rabi Hamiltonian (dots) are compared with perturbative expansion (lines). For numerical diagonalizations, the resonator Hilbert space is truncated to $n = 50$ Fock states.

where Ω, ω, and ϕ are the amplitude, the frequency, and the phase of the microwave drive, respectively. After successively applying the unitary transformations that diagonalize the qubit-resonator interaction $\mathcal{U}_1$ and the interaction between both qubits ($\mathcal{U}_2$ and $\mathcal{U}_3$), and switching to the rotating frame of both qubits and the resonator, we eventually obtain the following effective Hamiltonian after performing the RWA:

$$\begin{aligned}\mathcal{H}_{\circlearrowleft}^{\text{RWA}} &= \sum_{i=1,2} g_i(\gamma_i + \bar{\gamma}_i)\sigma_i^z\, a^\dagger a + J_{\text{res}}\,\sigma_1^z\sigma_2^z(2\,a^\dagger a + \mathbb{1}) \\ &\quad + \frac{\Omega(t)}{2}[\sin(2\theta_1) + \cos(2\theta_1)(-\gamma_1\gamma_2 + \bar{\gamma}_1\bar{\gamma}_2)][\mathrm{e}^{\mathrm{i}((\phi_1-\phi_2)-\varsigma\phi)}\sigma_1^+\sigma_2^- + \mathrm{e}^{-\mathrm{i}((\phi_1-\phi_2)-\varsigma\phi)}\sigma_1^-\sigma_2^+] \quad \text{if} \quad \omega = \omega_-, \\ \mathcal{H}_{\circlearrowleft}^{\text{RWA}} &= \sum_{i=1,2} g_i(\gamma_i + \bar{\gamma}_i)\sigma_i^z\, a^\dagger a + J_{\text{res}}\,\sigma_1^z\sigma_2^z(2\,a^\dagger a + \mathbb{1}) \\ &\quad + \frac{\Omega(t)}{2}[\sin(2\theta_2) + \cos(2\theta_2)(\gamma_1\bar{\gamma}_2 - \bar{\gamma}_1\gamma_2)][\mathrm{e}^{\mathrm{i}((\phi_1+\phi_2)-\phi)}\sigma_1^+\sigma_2^+ + \mathrm{e}^{-\mathrm{i}((\phi_1+\phi_2)-\phi)}\sigma_1^-\sigma_2^-] \quad \text{if} \quad \omega = \omega_+,\end{aligned} \tag{24}$$

where $\varsigma = \text{sign}(\Delta_1' - \Delta_2')$. We performed numerical calculations to confirm the validity of the above analytic expressions, and found a good agreement [see Fig. 3]. As expected, the process of parametric conversion between states $|{\downarrow\uparrow}\rangle$ and $|{\uparrow\downarrow}\rangle$ is favored when the ratio of the fixed transverse interaction mediated by the resonator J_{12}^{xx} to the detuning between the qubits $\hbar\omega_-$ is large [see Figs. 3(a) and 3(b) in the limit where ρ tends to 0]. Interestingly, the matrix elements associated with two-qubit parametric conversion are suppressed when the average detuning of the qubits with the resonator is reduced (i.e., $|\omega_r - \Delta|$), for moderate values of the detuning between qubits.

It is also worth noting that both types of parametric conversion between two-qubit states are strongly enhanced in the case where one of the two qubits is weakly detuned from the resonator and the microwave drive is applied to the other qubit [see Figs. 3(b) and 3(d) in the limit where ρ tends to 1]: an intuitive explanation is that in this configuration, the eigenstate corresponding to the weakly detuned qubit bears a large component of the resonator state in the bare basis, somehow

bringing this parametric conversion process effectively closer to a sideband transition. Ultimately, a compromise must be found between the detuning between qubits, and the detuning of each qubit from the resonator. If $\omega = \omega_-$ and $\phi = \varsigma(\phi_1 - \phi_2)$, we obtain the unitary evolution $e^{i\frac{\theta}{2}(\sigma_1^+\sigma_2^- + \sigma_1^-\sigma_2^+)}$, which can be used to define an iSWAP ($\theta = \pi$) or $\sqrt{\text{iSWAP}}$ gate ($\theta = \pi/2$).

Two-qubit parametric conversion has the disadvantage of requiring precise control over the phase ϕ of the applied microwave drive compared to the reference phases associated with the rotating frame of each qubit, which is a stringent practical constraint. Another feature to take into account is the presence of correlated errors in the two-qubit subspace: the combination of qubit relaxation and the transverse interaction mediated by the resonator introduces correlated bit-flip/phase-flip errors (i.e., ZX and XZ). Albeit rather negligible in general (as the mediated transverse interaction between both qubits tends to be small in the dispersive regime), this source of correlated errors may have to be taken into account in the limit where the two qubits are weakly detuned from each other, which is precisely the regime of interest for utilizing two-qubit parametric conversion (see Ref. [59] for details).

3. *Residual interactions*

One concern while developing a scalable architecture for quantum computation is the presence of residual $\sigma_z\sigma_z$ interactions between qubits in the fully diagonalized Hamiltonian: this type of interaction renders the resonant frequency of a physical qubit contingent on the state of the neighboring ones. We determine the value of this residual interaction for two qubits coupled to the same resonator in the case of the Jaynes-Cummings Hamiltonian by expanding the BCH formula up to fourth order (see Ref. [59] for details of the derivation):

$$J_{\text{res}} = \frac{1}{2}\,\gamma_1\,\gamma_2(g_1\,\gamma_2 + g_2\,\gamma_1). \tag{25}$$

For comparison purposes, we also determine the value of the residual interaction in the case of the Rabi Hamiltonian by expanding the BCH formula up to fourth order (see Ref. [59] for details of the derivation):

$$J_{\text{res}} = \frac{1}{2}(\gamma_1 + \bar{\gamma}_1)(\gamma_2 + \bar{\gamma}_2) \times \left\{[g_1(\gamma_2 - \bar{\gamma}_2) + g_2(\gamma_1 - \bar{\gamma}_1)] - \frac{g_1\,g_2}{\omega_r}\right\}. \tag{26}$$

We confirm the validity of the result given by this perturbative treatment with a numerical diagonalization [see Fig. 4]: we find good agreement, except when the resonant frequency of one of the qubits is close to the resonant frequency of the resonator. Interestingly, this parasitic interaction is relatively small in the dispersive regime as it occurs at the fourth order in the BCH expansion, which allows us to generate entanglement

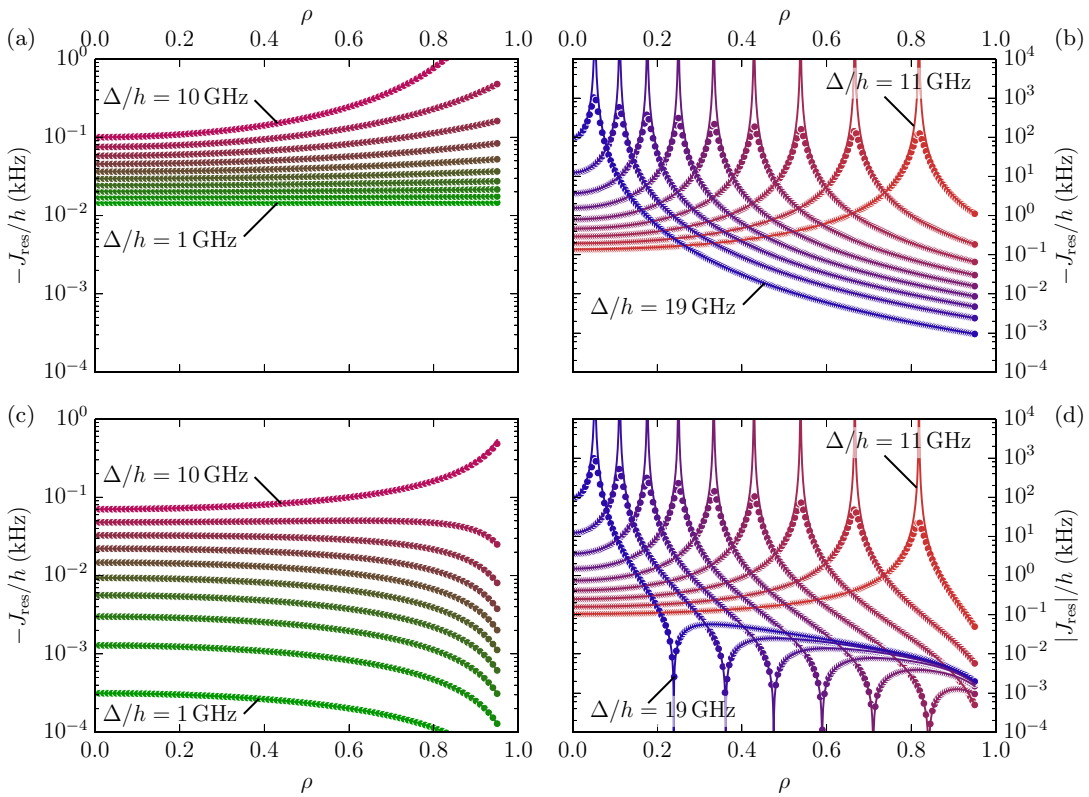

FIG. 4. (Color online) Residual $\sigma_z\sigma_z$ interaction between two qubits coupled to a common resonator (XcQED) for the Jaynes-Cummings Hamiltonian [(a) and (b)] and the Rabi Hamiltonian [(c) and (d)] vs the asymmetry ρ between their gap [$\Delta_1 = \Delta(1+\rho)$, $\Delta_2 = \Delta(1-\rho)$], for different values of $\Delta(\omega_r/h = 20\ \text{GHz}, g_1/h = g_2/h = 100\ \text{MHz})$: results obtained from numerical diagonalization (dots) are compared with perturbative expansion (lines). In (a) and (c), Δ/h ranges from 1 to 10 GHz in steps of 1 GHz, whereas for (b) and (d), Δ/h ranges from 11 to 19 GHz in steps of 1 GHz. For numerical diagonalizations, the resonator Hilbert space is truncated to $n = 40$ Fock states.

via two-qubit parametric conversion with a relatively large ON/OFF ratio (see Sec. II B 2). The main difference between the Jaynes-Cummings and Rabi models is qualitative in nature. In the case of the Rabi Hamiltonian, the residual interaction J_{res} can be exactly canceled if the detunings between the resonant frequencies of the two qubits and the frequency of the resonator have opposite signs, as can be seen in Fig. 4(d).

C. Implementation of a 2D nearest-neighbor quantum architecture

We consider the possibility of devising a quantum register wherein physical qubits are disposed on a 2D square lattice, and each pair of nearest-neighbors are transversely coupled to a common resonator: if all physical qubits are biased at their symmetry point, the static Hamiltonian of the entire quantum register remains parity-conserving. We presented two different ways to generate entanglement between two qubits in this configuration, which are relatively insensitive to cross-talk, thus simplifying their operation compared with cross-resonance. Driving qubits along their longitudinal degree of freedom allows us to induce transitions between states of same parity, while operating the physical qubits at their symmetry point.

The justification of the RWA for either the transverse or the longitudinal drive of each physical qubit (i.e., for single- and two-qubit gates, respectively) is an essential issue which must be examined minutely. The RWA sets an upper bound on the speed at which the state of the quantum register can be manipulated. Parity conservation allows us to significantly restrict the number of parametric conversion and cross-resonance-like processes that must be taken into account in this analysis. Furthermore, most of these higher-order processes can be easily neglected, as their corresponding matrix elements are small in the dispersive regime, according to the order in which they occur in the expansion of the BCH formula. We do not detail the conditions for the validity of the RWA here, as we prefer to exemplify their derivation in the case in which each artificial atom is longitudinally coupled to the resonators surrounding it (ZcQED), which is a slightly more intricate configuration, as all higher-order sideband transitions are allowed, owing to the absence of a parity selection rule (see Sec. III C 3).

Conversely, residual interactions lead to a constant accumulation of spurious phase, which degrades the fidelity of the targeted unitary evolution, and, in so doing, sets a lower bound on the speed of single- and two-qubit gates in order to maintain the related infidelity below a certain level in the error budget set by the accuracy threshold. We derive analytic expressions based on a perturbative expansion for each of the relevant quantities (i.e., the dispersive shift in the case of sideband transitions and residual $\sigma_z\sigma_z$ interactions in the case of two-qubit parametric conversion), which are applicable for the dispersive regime. Besides enabling certain transitions (namely blue sideband transitions, and the $|00\rangle \leftrightarrow |11\rangle$ transition in the case of two-qubit parametric conversion), taking the nonsecular term in the interaction between qubits and resonators into account provides a more accurate quantitative estimate of these residual interactions.

The existence of matrix elements is not sufficient to assess whether a given type of tunable interaction is useful or not. Ultimately, the choice of the parameters is a trade-off between the upper and lower bounds, as there must be an operating range for the amplitude of the applied microwave drive, which is compatible with both constraints. Following this line of reasoning, two-qubit parametric conversion offers more flexibility, as residual $\sigma_z\sigma_z$ interactions occur at fourth order in the expansion of the BCH formula, whereas the dispersive shift occurs at second order; however, the justification of the RWA is more intricate in the case of two-qubit parametric conversion, as it requires the application of microwave drives with larger amplitudes compared with sideband transitions in order to obtain the same gate speed.

A rather favorable regime in that sense is to operate the system in the limit of large qubit-resonator detuning, and small qubit-qubit detuning, wherein the matrix elements corresponding to two-qubit parametric conversion via the $|01\rangle \leftrightarrow |10\rangle$ transition are large [see the limit $\rho \to 0$ in Figs. 3(a) and 3(b)] and the residual $\sigma_z\sigma_z$ interactions remain small [see Fig. 4], though it renders the quantum register more sensitive to cross-talk while performing single-qubit gates. Moreover, the detuning between any given qubit in the lattice and its four nearest-neighbors should be properly adjusted so that entanglement generation via two-qubit parametric conversion remains frequency-selective for a targeted pair of qubits. Interestingly, a large detuning between each qubit and the resonator enables larger matrix elements for this process of two-qubit parametric conversion. This encourages the utilization of very high-frequency resonators to mediate the interactions between each pair of nearest-neighbors in order to allow larger detunings between the two qubits. In the limit where one of the two qubits is weakly detuned from the resonator, the justification of the RWA for two-qubit parametric conversion is intrinsically limited by the proximity of sideband transitions in the frequency spectrum, albeit the related matrix elements can be relatively large [see the limit $\rho \to 1$ in Figs. 3(b) and 3(d)]: this regime also enhances the residual $\sigma_z\sigma_z$ interactions, and the role of the Purcell effect.

Sideband transitions remain an attractive route for entanglement generation, as the justification of the RWA offers an increased flexibility on the choice of the amplitude of the applied microwave drive and the relative detuning between each pair of physical qubits situated on a given vertex of the lattice. Without the limitation set by the presence of residual interactions, they would allow faster two-qubit gates and reduced risk of cross-talk. In the next section, we will present an approach which enables a significant improvement of their performance by suppressing the dispersive shift, the Purcell effect, and correlated errors in the two-qubit subspace (i.e., ZX and XZ errors). This alternate approach releases the restrictions inherent to the dispersive regime on the various energy scales involved, thus allowing us to take advantage of the large coupling strengths that can be achieved with Josephson-junction-based qubits.

III. LONGITUDINAL COUPLING BETWEEN QUBIT AND RESONATOR (ZcQED)

We wish to introduce an alternative layout for circuit QED, wherein a qubit is coupled to a quantum harmonic oscillator via its longitudinal degree of freedom (i.e., along σ_z); we

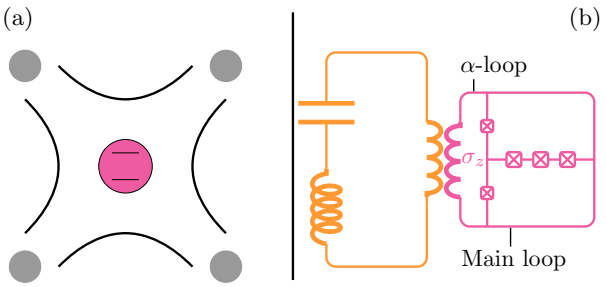

FIG. 5. (Color online) (a) Schematic representation of a single ion confined in a linear quadrupole RF trap: the oscillator corresponds to the quantized center-of-mass motion of the ion in the trap (not represented). (b) Possible implementation of a ZcQED experiment with a flux qubit: the coupling to the longitudinal degree of freedom of the artificial atom can be achieved by inductively coupling the resonator to the α-loop of the qubit (see Appendix A 1).

call this layout ZcQED [see Fig. 5(b)]. Such an approach has a few significant advantages over XcQED, such as the nonoccurrence of dispersive shift (which allows to recover scalable sideband transitions) and the absence of the Purcell effect. The analogy with trapped ions will become clear when considering the transverse microwave drive of the qubit. Besides the possibility of realizing single-qubit operations, we will also find every possible sideband transition with the same nonlinear dependence of their respective effective Rabi frequencies as a function of the Fock state of the resonator [73,74]. However, the origins of sideband transitions in these cases are essentially different: in ZcQED, a fixed qubit-resonator interaction is required to find the matrix elements for these tunable interactions, whereas in ion traps, this mechanism is provided by the recoil momentum of the atom under laser irradiation [75] [see Fig. 5(a)].

Wang *et al.* discussed the possibility of realizing tunable interactions between two qubits which are longitudinally coupled to the same resonator [76]: the residual $\sigma_z\sigma_z$ interactions in the static Hamiltonian are canceled by operating the qubits at a bias point at which their longitudinal coupling with the resonator is zero, and the interaction can be turned on by simultaneously applying dc pulses that make the longitudinal coupling between each qubit and the resonator nonzero. Kerman examined a similar configuration in the limit where the resonator can be treated classically [77], and drew an analogy with trapped ions, which he used to devise tunable two-qubit interactions based on spin-dependent forces [31,78–83]. In this section, we will develop a different approach, based on sideband transitions. For this purpose, we will strictly restrict ourselves to the quantum limit ($\omega_r \gg k_B T$, where k_B is the Boltzmann constant and T is the temperature) in order to avoid thermal population of the resonator excited states.

A. Single-qubit case

1. Static Hamiltonian

The Hamiltonian of a qubit longitudinally coupled to a quantum harmonic oscillator reads

$$\mathcal{H} = \omega_r\, a^\dagger a + \frac{\Delta}{2}\,\sigma_z + g\,\sigma_z(a^\dagger + a), \tag{27}$$

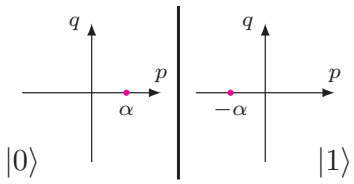

FIG. 6. (Color online) Schematic representation of the effect of the coupling of a single qubit to the resonator in phase space within the framework of ZcQED. The amplitude of the effective displacement $|\alpha|$ due to the coupling does not depend upon the state of the qubit, which explains why there are no dispersive or Lamb shifts.

where ω_r is the harmonic oscillator resonant frequency, Δ is the qubit resonant frequency, and g is the qubit-oscillator coupling strength. Conversely, the Hamiltonian that accounts for the interaction between the atom and the resonator is not parity-conserving in ZcQED, as the coupling term does not commute with the parity operator Π: this implies that no transition is *a priori* forbidden by the parity selection rule, which is a direct consequence of coupling the atom via its longitudinal degree of freedom. This Hamiltonian can be exactly diagonalized via a Lang-Firsov unitary transformation [84]

$$\mathcal{U} = \exp[-\theta\,\sigma_z(a^\dagger - a)], \tag{28}$$

where $\theta = g/\omega_r$. The fully diagonalized Hamiltonian is written as

$$\mathcal{H}' = \omega_r\, a^\dagger a + \frac{\Delta}{2}\,\sigma_z - \frac{g^2}{\omega_r}\,\mathbb{1}. \tag{29}$$

Remarkably, the parameters of the atomic and photonic degrees of freedom are not modified by the diagonalization of the coupling term (i.e., the absence of Lamb shift). All we observe is a renormalization of the energy associated with zero-point fluctuations, and the absence of dispersive shift as indicated above. This result can be understood very intuitively by considering a phase space representation of the oscillator [see Fig. 6]: depending on whether the qubit is in its ground or excited state, it exerts a displacement in phase space on the resonator of the same amplitude $|\alpha| = g$ in opposite directions. It is precisely this displacement α which is responsible for the renormalization of the zero-point energy going as $|\alpha|^2/\omega_r$: as the amplitude of the displacement does not depend on the qubit state, there is thus no dispersive shift.

This may appear to be a disadvantage, as the resonant frequency of the resonator being independent of the qubit state, it precludes to perform dispersive readout of the qubit state. However, from the point of view of quantum computation, the absence of residual coupling between the qubit and the resonator in this configuration allows us to use sideband transitions to generate entanglement, as the qubit is not affected by the number of excitations in the resonator. At this point, one can easily foresee the benefit of this type of interaction for the development of a scalable architecture for quantum information processing based on superconducting qubits: however, it remains to be guaranteed that residual $\sigma_z\sigma_z$ interactions between two qubits can be exactly canceled in the case where two qubits are coupled to the same resonator. Before clarifying this issue, let us see first what type of

tunable interactions can be realized by driving the qubit with a transverse microwave drive.

2. *Transverse microwave drive of the qubit*

Let us consider that one applies a transverse microwave drive to the qubit: this can be achieved by driving the flux through the main loop of the qubit [see Fig. 5(b)]. The corresponding time-dependent Hamiltonian thus reads

$$\mathcal{H}(t) = \mathcal{H} + \Omega(t)\cos(\omega t + \phi)\sigma_x, \tag{30}$$

where $\mathcal{H}$ is given by Eq. (27), and Ω, ω, and ϕ are, respectively, the amplitude, the frequency, and the phase of the microwave drive. After applying the Lang-Firsov unitary transformation mentioned above, we obtain the following time-dependent Hamiltonian:

$$\mathcal{H}'(t) = \mathcal{H}' + \Omega(t)\cos(\omega t + \phi)\exp\left[-\frac{1}{2}\left(\frac{2g}{\omega_r}\right)^2\right] \times\left[\sigma_+ \exp\left(\frac{2g}{\omega_r}a^\dagger\right)\exp\left(-\frac{2g}{\omega_r}a\right) + \sigma_- \exp\left(-\frac{2g}{\omega_r}a^\dagger\right)\exp\left(\frac{2g}{\omega_r}a\right)\right], \tag{31}$$

where $\mathcal{H}'$ is given by Eq. (29). We will denote the Debye-Waller factor by $\mathcal{D}$:

$$\mathcal{D} = \exp\left[-\frac{1}{2}\left(\frac{2g}{\omega_r}\right)^2\right]. \tag{32}$$

In order to switch to the rotating frame of the qubit and the resonator, we apply the following time-dependent unitary transformation:

$$\mathcal{U} = \exp\left[-\mathrm{i}\frac{(\Delta t + \phi_q)}{2}\sigma_z - \mathrm{i}(\omega_r t + \phi_r)a^\dagger a\right], \tag{33}$$

where ϕ_q and ϕ_r are the reference phases of the rotating frame of the qubit and the resonator, respectively.

We obtain the time-dependent Hamiltonian:

$$\mathcal{H}''(t) = \Omega(t)\cos(\omega t + \phi)\mathcal{D}\left\{\mathrm{e}^{\mathrm{i}(\Delta t+\phi_q)}\sigma_+ \exp\left[\frac{2g}{\omega_r}\mathrm{e}^{\mathrm{i}(\omega_r t+\phi_r)}a^\dagger\right]\exp\left[-\frac{2g}{\omega_r}\mathrm{e}^{-\mathrm{i}(\omega_r t+\phi_r)}a\right] + \mathrm{e}^{-\mathrm{i}(\Delta t+\phi_q)}\sigma_- \exp\left[-\frac{2g}{\omega_r}\mathrm{e}^{\mathrm{i}(\omega_r t+\phi_r)}a^\dagger\right]\exp\left[\frac{2g}{\omega_r}\mathrm{e}^{-\mathrm{i}(\omega_r t+\phi_r)}a\right]\right\}. \tag{34}$$

Let us first examine how to implement single-qubit operations (i.e., $\omega = \Delta/\hbar$). Within the RWA, the effective Hamiltonian is found to be

$$\mathcal{H}_{\mathrm{sq}}^{\mathrm{RWA}} = \frac{\Omega(t)}{2}\mathcal{D}\left[\sum_{\ell=0}^{\infty}\frac{(-1)^\ell}{(\ell!)^2}\left(\frac{2g}{\omega_r}\right)^{2\ell} a^{\dagger\ell}a^\ell(\mathrm{e}^{\mathrm{i}(\phi_q-\phi)}\sigma_+ + \mathrm{e}^{-\mathrm{i}(\phi_q-\phi)}\sigma_-)\right]. \tag{35}$$

Setting the phases ϕ_q and ϕ equal to zero, one can show that the matrix elements corresponding to single-qubit operations depending on the Fock state of the resonator are given by

$$\langle n,\uparrow|\mathcal{H}_{\mathrm{sq}}^{\mathrm{RWA}}|n,\downarrow\rangle = \frac{\Omega}{2}\mathcal{D}\,\mathrm{L}_n\left[\left(\frac{2g}{\omega_r}\right)^2\right], \tag{36}$$

where $\mathrm{L}_n(x)$ is a Laguerre polynomial of degree n. The photon state dependence of the latter matrix elements requires the system to be operated in the quantum limit. Thermal population of the resonator excited states would inevitably entangle the qubit and the resonator when one intends to perform single-qubit operations with a resonant microwave drive ($\omega = \Delta/\hbar$). Another reason why we need to suppress thermal excitations in the resonator is that all of the operations that we need to implement in this proposal, whether two-qubit operations or readout, rely on sideband transitions. This is in stark contrast to the work of Kerman, which is based on spin-dependent forces [77]. Generally speaking, the effect of thermal excitations is completely negligible in the temperature range at which this type of system is operated (as an example, a resonator with a resonant frequency $\omega_r/h = 2$ GHz at a temperature of $T = 10$ mK gives a Boltzmann factor $\mathrm{e}^{-\beta\omega_r} = 7\times10^{-5}$). Considering the typical energy scales involved in superconducting qubits, an advantage of ZcQED over trapped ions is that the initialization of the quantum register does not require sideband cooling [85].

Let us consider now how to realize red and blue sideband transitions of order k [i.e., $\omega = |\Delta - k\,\omega_r|/\hbar$ and $\omega = (\Delta + k\,\omega_r)/\hbar$, respectively]. Within the RWA, the corresponding effective Hamiltonians read

$$\begin{aligned}\mathcal{H}_{\mathrm{red}}^{\mathrm{RWA}} &= \frac{\Omega(t)}{2}\mathcal{D}\left\{\sum_{\ell=0}^{\infty}\frac{(-1)^{\ell+k}}{\ell!\,(\ell+k)!}\left(\frac{2g}{\omega_r}\right)^{2\ell+k}[\mathrm{e}^{\mathrm{i}((\phi_q-k\,\phi_r)-\varsigma\phi)}\sigma_+a^{\dagger\ell}a^{\ell+k} + \mathrm{e}^{-\mathrm{i}((\phi_q-k\,\phi_r)-\varsigma\phi)}\sigma_-a^{\dagger\ell+k}a^\ell]\right\},\\ \mathcal{H}_{\mathrm{blue}}^{\mathrm{RWA}} &= \frac{\Omega(t)}{2}\mathcal{D}\left\{\sum_{\ell=0}^{\infty}\frac{(-1)^{\ell}}{\ell!\,(\ell+k)!}\left(\frac{2g}{\omega_r}\right)^{2\ell+k}[\mathrm{e}^{\mathrm{i}((\phi_q+k\,\phi_r)-\phi)}\sigma_+a^{\dagger\ell+k}a^{\ell} + \mathrm{e}^{-\mathrm{i}((\phi_q+k\,\phi_r)-\phi)}\sigma_-a^{\dagger\ell}a^{\ell+k}]\right\},\end{aligned} \tag{37}$$

where $\varsigma = \mathrm{sign}(\Delta - k\,\omega_r)$. Setting all the phases equal to zero for the sake of simplicity, one can determine the matrix elements associated with these various processes:

$$\begin{aligned}\langle n+k,\downarrow|\mathcal{H}_{\mathrm{red}}^{\mathrm{RWA}}|n,\uparrow\rangle &= \frac{\Omega}{2}\,\mathcal{D}\left(-\frac{2\,g}{\omega_r}\right)^k\sqrt{\frac{n!}{(n+k)!}}\,\mathrm{L}_n^k\left[\left(\frac{2\,g}{\omega_r}\right)^2\right],\\ \langle n+k,\uparrow|\mathcal{H}_{\mathrm{blue}}^{\mathrm{RWA}}|n,\downarrow\rangle &= \frac{\Omega}{2}\,\mathcal{D}\left(\frac{2\,g}{\omega_r}\right)^k\sqrt{\frac{n!}{(n+k)!}}\,\mathrm{L}_n^k\left[\left(\frac{2\,g}{\omega_r}\right)^2\right],\end{aligned} \tag{38}$$

where $\mathrm{L}_n^k(x)$ is an associated Laguerre polynomial. We find a set of sideband transitions which couple states of arbitrary parity, since the static Hamiltonian is not parity-conserving. Some differences compared with the situation encountered in XcQED can be pointed out. First of all, the resonance conditions for performing single-qubit operations and sideband transitions do not depend on the photon state of the resonator in ZcQED, due to the absence of dispersive shift. Moreover, their respective matrix elements strongly depend on the resonator state, as can be seen in the expressions given above. Naturally, the matrix elements corresponding to sideband transitions always depend on the photon state of the resonator, merely because $\langle n+1|a^\dagger|n\rangle = \langle n|a|n+1\rangle = \sqrt{n+1}$: the enhanced dependence versus n originates from the associated Laguerre polynomials. Schematically, in XcQED, the nonlinearity is entirely contained within the energy spectrum (the so-called *nonlinear Jaynes-Cummings ladder* [86]), whereas in ZcQED, it manifests itself in the tunable interactions. This result is akin to what is found in trapped ion systems [73], further referred to as the *nonlinear Jaynes-Cummings model* [74]. This nonlinearity is fully characterized by the Lamb-Dicke parameter η, which in ion traps is defined by

$$\eta = (k\cos\theta)\sqrt{\frac{\hbar}{2\,m\,\omega_x}}, \tag{39}$$

where $(k\cos\theta)$ is the projection of the wave vector of the laser field onto the motional axis, m is the mass of the ion, and ω_x is the trap frequency. Ion traps are usually operated in the Lamb-Dicke regime ($\eta \ll 1$), which is less sensitive to nonlinear effects. In ZcQED, the role of the Lamb-Dicke parameter is played by the ratio $(2\,g/\omega_r)$. The possibility of achieving a rather large atom-photon coupling g guarantees rather fast single-qubit and two-qubit operations at the expense of enhanced sensitivity of the matrix elements related to the sideband transitions as functions of the resonator state. This nonlinear behavior has been used on purpose in ion traps for determination of the motional state of the ion (see, for example, Refs. [87,88]). From the point of view of quantum computation, this nonlinearity places restrictions on the manipulation of quantum states, especially when it comes to the generation of entanglement via sideband transitions: one of our aims hereafter will be to conceive of interactions that allow us to circumvent this issue in order to avoid the generation of spurious entanglement between the qubits and the resonators mediating the interactions, and by so doing, to avert the leakage of information out of the computational subspace.

3. *Qubit relaxation*

We will denote by $1/\gamma_{\mathrm{q}}$ the qubit lifetime, and by $1/\kappa$ the photon lifetime of the resonator. The eigenstates of the coupled qubit-resonator system $|\overline{n,\psi}\rangle$ can be expressed as functions of the bare states $|n,\psi\rangle$ as follows:

$$|\overline{n,\psi}\rangle = \mathcal{U}|n,\psi\rangle = \exp[-\theta\,\sigma_z(a^\dagger - a)]|n,\psi\rangle, \tag{40}$$

where $|n\rangle$ is a given Fock state of the resonator, $|\psi\rangle$ is an arbitrary qubit state, and $\theta = g/\omega_r$ [see Eq. (28)]. The photon state dependent qubit relaxation rate $\Gamma_{\gamma_{\mathrm{q}}}^{\mathrm{q},n}$ is given by

$$\begin{aligned}\Gamma_{\gamma_{\mathrm{q}}}^{\mathrm{q},n} &= \gamma_{\mathrm{q}}|\langle\overline{n,\downarrow}|\sigma_-|\overline{n,\uparrow}\rangle|^2\\ &= \gamma_{\mathrm{q}}|\langle n,\downarrow|\mathcal{U}^\dagger\sigma_-\,\mathcal{U}|n,\uparrow\rangle|^2.\end{aligned} \tag{41}$$

After expansion of the BCH formula, it can be shown that

$$\mathcal{U}^\dagger\sigma_-\,\mathcal{U} = \sigma_-\exp[-2\,\theta(a^\dagger - a)]. \tag{42}$$

Eventually, the qubit relaxation rate reads

$$\Gamma_{\gamma_{\mathrm{q}}}^{\mathrm{q},n} = \gamma_{\mathrm{q}}\,\mathcal{D}^2\left\{\mathrm{L}_n\left[\left(\frac{2\,g}{\omega_r}\right)^2\right]\right\}^2. \tag{43}$$

Hence, the spontaneous emission rate of the atom can either be enhanced or inhibited compared with what it would be if the oscillator was in its ground state, depending on the state of the latter and regardless of the detuning between them. This result is consistent with the dependence found for the matrix elements corresponding to single-qubit operations A_{sq}^n as a function of n [see Eq. (36)]. This situation is significantly different from what is encountered in the dispersive regime of XcQED [89]. Moreover, the expression for the qubit lowering operator σ_- in its rotated form reveals the presence of correlated errors which correspond to the simultaneous relaxation of the qubit state and either the relaxation of a Fock state $|n\rangle$ to $|n-k\rangle$, or the excitation of a Fock state $|n\rangle$ to $|n+k\rangle$ if $(\Delta - k\,\omega_r) > 0$. Similarly to the case of single-qubit errors, the error rates associated with these correlated errors depend on the Fock state of the resonator, and they are given by

$$\begin{aligned}\Gamma_{\gamma_{\mathrm{q}}}^{\mathrm{q},n,-k} &= \gamma_{\mathrm{q}}|\langle\overline{n-k,\downarrow}|\sigma_-|\overline{n,\uparrow}\rangle|^2\\ &= \gamma_{\mathrm{q}}|\langle n-k,\downarrow|\mathcal{U}^\dagger\sigma_-\,\mathcal{U}|n,\uparrow\rangle|^2\\ &= \gamma_{\mathrm{q}}\,\mathcal{D}^2\left(\frac{2\,g}{\omega_r}\right)^{2k}\frac{(n-k)!}{n!}\left\{\mathrm{L}_{n-k}^k\left[\left(\frac{2\,g}{\omega_r}\right)^2\right]\right\}^2,\\ \Gamma_{\gamma_{\mathrm{q}}}^{\mathrm{q},n,+k} &= \gamma_{\mathrm{q}}|\langle\overline{n+k,\downarrow}|\sigma_-|\overline{n,\uparrow}\rangle|^2\\ &= \gamma_{\mathrm{q}}|\langle n+k,\downarrow|\mathcal{U}^\dagger\sigma_-\,\mathcal{U}|n,\uparrow\rangle|^2\\ &= \gamma_{\mathrm{q}}\,\mathcal{D}^2\left(\frac{2\,g}{\omega_r}\right)^{2k}\frac{n!}{(n+k)!}\left\{\mathrm{L}_n^k\left[\left(\frac{2\,g}{\omega_r}\right)^2\right]\right\}^2.\end{aligned} \tag{44}$$

Similarly to residual $\sigma_z\sigma_z$ interactions, the occurrence of these correlated errors is intrinsically related to the presence of fixed interactions. This feature is specific to ZcQED. The

influence of these correlated errors may not be negligible in the limit where the Lamb-Dicke parameter η is not small, especially when they arise at the lowest order: the case corresponding to $k = 1$ is particularly relevant in the context of entanglement generation via sideband transitions.

Besides the dispersive shift, an undesirable consequence of the coupling between the transverse degrees of freedom of both the qubit and the resonator in XcQED is that it makes the qubit lifetime dependent on the photon lifetime in the resonator (the so-called *Purcell effect* [48]). The Purcell contribution to the qubit relaxation rate in XcQED is given by $\Gamma_\kappa^{q,0} = \kappa\, g^2/(\Delta - \omega_r)^2$ in the dispersive regime. Kleppner discussed how the Purcell effect can be used to purposely inhibit the spontaneous emission of an atom by placing it inside a cavity with a proper detuning condition [90]. Enhanced and inhibited spontaneous emissions have been observed in different contexts, either in atomic systems (such as a single electron in a Penning trap [91] or Rydberg atoms in a cavity [92,93]) or in solid-state devices (such as quantum dots [94] and superconducting qubits [49]). Various strategies exist to counteract the Purcell effect, either by engineering the electromagnetic environment (*Purcell filter* [95]) or by encoding the information in a decoherence-free subspace (*Purcell protected qubit* [96]). Hereafter, we will establish the effect of a finite photon lifetime on the qubit relaxation rate in ZcQED. The Purcell contribution $\Gamma_\kappa^{q,n}$ to the spontaneous emission rate of the artificial atom can be found based on Fermi's golden rule [90]:

$$\begin{aligned}\Gamma_\kappa^{q,n} &= \kappa\,|\langle \overline{n,\downarrow}|a|\overline{n,\uparrow}\rangle|^2 \\ &= \kappa\,|\langle n,\downarrow|\mathcal{U}^\dagger a\,\mathcal{U}|n,\uparrow\rangle|^2. \end{aligned} \tag{45}$$

Expanding the BCH formula, we obtain

$$\mathcal{U}^\dagger a\,\mathcal{U} = a - \theta\,\sigma_z. \tag{46}$$

The Purcell relaxation rate thus reads as follows:

$$\Gamma_\kappa^{q,n} = \kappa\,|\langle n,\downarrow|a - \theta\,\sigma_z|n,\uparrow\rangle|^2 = 0. \tag{47}$$

Accordingly, the finite photon lifetime $1/\kappa$ has no bearing on the qubit relaxation rate, irrespective of the state of the resonator. This is a direct consequence of coupling the atom via its longitudinal degree of freedom. Absence of the Purcell effect stands as another valuable feature of ZcQED.

B. Two qubits coupled to a single resonator via the same degree of freedom [Z*pp*Z]

We will first consider the case of two qubits that are coupled longitudinally to a bosonic mode via the same degree of freedom, say, for example, two flux qubits coupled inductively via their α-loop to a lumped element resonator. Such a system is well described by the following Hamiltonian:

$$\mathcal{H} = \omega_r\, a^\dagger a + \sum_{i=1,2}\left[\frac{\Delta_i}{2}\,\sigma_i^z + g_i\,\sigma_i^z(a^\dagger + a)\right]. \tag{48}$$

This Hamiltonian can also be exactly diagonalized via a Lang-Firsov unitary transformation

$$\mathcal{U} = \exp\left[-\sum_{i=1,2}\theta_i\,\sigma_i^z(a^\dagger - a)\right], \tag{49}$$

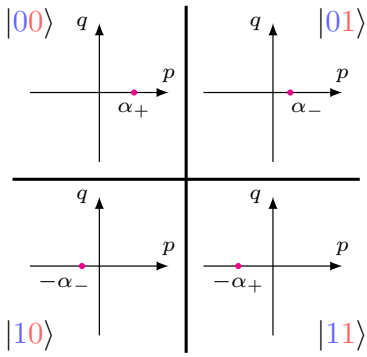

FIG. 7. (Color online) Schematic representation of the effect of the coupling to two qubits on the resonator in phase space [Z*pp*Z configuration]: the amplitude of the effective displacement $|\alpha|$ due to the coupling depends on the state of the qubits ($\alpha_+ = (g_1 + g_2)$ and $\alpha_- = (g_1 - g_2)$), which explains the presence of the residual $\sigma_z\sigma_z$ interaction.

where $\theta_i = g_i/\omega_r$. After expanding the BCH formula up to the second order, the fully diagonalized Hamiltonian is found to be

$$\mathcal{H}' = \omega_r\, a^\dagger a + \sum_{i=1,2}\frac{\Delta_i}{2}\,\sigma_i^z - \frac{2\,g_1\,g_2}{\omega_r}\,\sigma_1^z\sigma_2^z - \frac{g_1^2 + g_2^2}{\omega_r}\,\mathbb{1}. \tag{50}$$

Again, the typical energy scales of the resonator and both qubits are not renormalized by the coupling, and there is no dispersive shift; however, one significant term besides the renormalization of the zero-point energy is the presence of a residual $\sigma_z\sigma_z$ interaction term between both qubits. Similarly to the single qubit case, this outcome can be explained by considering a phase space representation of the oscillator [see Fig. 7]. If the qubits are in states $|00\rangle$ or $|11\rangle$, they displace the resonator state by $\pm\alpha_+$, where $\alpha_+ = (g_1 + g_2)$, whereas if the qubits are in states $|01\rangle$ or $|10\rangle$, they displace the resonator state by $\pm\alpha_-$, where $\alpha_- = (g_1 - g_2)$, causing the zero-point energy to be renormalized as $(g_1 + g_2)^2/\omega_r$ and $(g_1 - g_2)^2/\omega_r$, respectively. Consequently, there is in average a renormalization of the zero-point energy that behaves as $(g_1^2 + g_2^2)/\omega_r$, and a qubit state-dependent part that behaves as $2\,g_1\,g_2/\omega_r$. This latter contribution is responsible for the residual $\sigma_z\sigma_z$ interaction that appears in the fully diagonalized Hamiltonian. As opposed to what is encountered in XcQED, where this type of residual interaction occurs at the fourth order, in the case of ZcQED, it occurs at the second order.

For typical parameters, if g_1/h and g_2/h are of the order of a few hundreds of MHz and if ω_r/h is of the order of a few GHz, this means that these residual interactions between atomic degrees of freedom can be of the order of few tens of MHz. This results in rather low ON/OFF ratios, which render this type of layout unsuitable for the manipulation of quantum states. This result is fundamentally different from what is encountered in the case of trapped ions. Indeed, in ZcQED, sideband transitions are supported by the fixed interaction between the artificial atom and the resonator, whereas in ion traps they occur based on the recoil momentum of the

atom caused by photon absorption. It is the presence of these fixed interactions that is responsible for the residual $\sigma_z\sigma_z$ interactions, and makes the situation for solid-state devices substantially different from that for atomic systems. Another noticeable difference from XcQED is the fact that this residual interaction does not depend on the detuning between the qubit and the resonator, as both systems do not exchange photons.

We looked for a way to overcome this limitation in order to have *well-characterized qubits*, a necessary requirement for the development of a scalable architecture. We thus examined two alternatives, wherein a pair of physical qubits are coupled either via one resonator through orthogonal degrees of freedom, or via two resonators fixedly coupled through the same degree of freedom, which we denote as Z*pq*Z and Z*p(pp)p*Z, respectively. The former does not provide *a "universal" set of quantum gates*, while the latter is not free of residual $\sigma_z\sigma_z$ interactions (see Ref. [59] for details).

C. Two qubits coupled through two resonators via alternating degrees of freedom [Z*p(qq)p*Z]

The architecture that we are considering is described in Fig. 8(a): for every pair of nearest-neighboring qubits, each qubit is coupled to a distinct resonator via a given degree of freedom, and both resonators are coupled through an orthogonal degree of freedom. Based on our idea for developing an architecture for flux qubits, this means that each flux qubit would be coupled inductively to a resonator, and that each pair of resonators would be coupled capacitively.

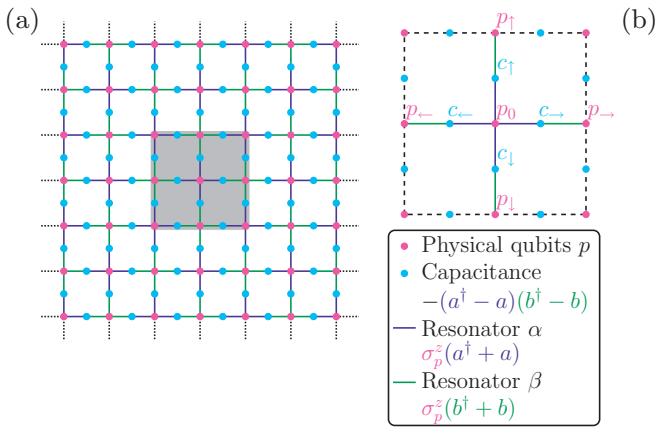

FIG. 8. (Color online) (a) Schematic representation of an array of qubits on a 2D square lattice where coupling is mediated by two resonators fixedly coupled [Z*p(qq)p*Z configuration]. (b) Schematic representation of an enlarged unit cell among the 2D array: each physical qubit (say p_0 at the center) is surrounded by eight resonators, thereby complicating the justification of the rotating wave approximation for single-qubit operations and sideband transitions.

1. *Static Hamiltonian*

The Hamiltonian describing this type of unit cell coupling two neighboring qubits reads as follows:

$$\mathcal{H} = \omega_1\, a^\dagger a + \omega_2\, b^\dagger b + \sum_{i=1,2} \frac{\Delta_i}{2}\,\sigma_i^z + g_1\,\sigma_1^z(a^\dagger + a) + g_2\,\sigma_2^z(b^\dagger + b) - g_c(a^\dagger - a)(b^\dagger - b), \tag{51}$$

where g_1 and g_2 are the coupling between qubit 1 and resonator α and qubit 2 and resonator β, respectively, and g_c is the coupling between resonator α and resonator β. This Hamiltonian can be exactly diagonalized following the method shown in Appendix B, which eventually gives the fully diagonal Hamiltonian

$$\mathcal{H}' = \omega_+\, a^\dagger a + \omega_-\, b^\dagger b + \sum_{i=1,2} \frac{\Delta_i}{2}\,\sigma_i^z - \left(\frac{g_1^2}{\omega_1} + \frac{g_2^2}{\omega_2}\right)\mathbb{1}, \tag{52}$$

where $\omega_\pm$ are the resonant frequencies of two fixedly coupled resonators [see Eq. (B9)]. This system is thus free of any type of residual coupling, whether between atomic degrees of freedom (residual $\sigma_z\sigma_z$ interactions), between atomic and photonic degrees of freedom (dispersive shift), or between photonic degrees of freedom (self-Kerr or cross-Kerr nonlinearities). Such a type of unit cell provides well-defined qubits allowing reliable single-qubit operations, and well-defined bosonic modes allowing reliable two-qubit operations via sideband transitions. As the coupling term between a given qubit and any of the four nearest-neighbor resonators commutes with the free Hamiltonian of the qubit and the coupling terms with the three other nearest-neighbor resonators, the good features exhibited in this configuration at the level of one unit cell will remain valid within a 2D array. This is another noteworthy advantage of coupling qubits via their longitudinal degree of freedom, which ensures the modularity of this coupling scheme. This is in stark contrast with the situation encountered in XcQED wherein the coupling terms do not commute with the free Hamiltonian of the physical qubits.

Below, we will determine how sideband transitions between each qubit and the two resonators can be operated and used to generate entanglement and perform readout. The main asset of ZcQED over trapped ions remains the possibility of achieving rather strong couplings between the atomic and photonic degrees of freedom, thereby enhancing the matrix elements associated with sideband transitions and accelerating the speed of various possible operations. However, working out of the Lamb-Dicke regime brings some additional difficulties related to the nonlinearity of the Jaynes-Cummings model. In the following, we will show how to overcome these limitations.

2. *Transverse microwave drive of one qubit*

Assuming that a transverse microwave drive is applied to the first qubit, the time-dependent Hamiltonian is given by

$$\mathcal{H}(t) = \mathcal{H} + \Omega(t)\cos(\omega t)\,\sigma_1^x, \tag{53}$$

where $\mathcal{H}$ is given by Eq. (51), and Ω and ω are, respectively, the amplitude and the frequency of the microwave drive. After successively applying the same set of unitary transformations

used to diagonalize the static Hamiltonian (see Appendix B), the time-dependent Hamiltonian reads

$$\mathcal{H}'(t) = \mathcal{H}' + \Omega(t)\cos(\omega t)\,\exp\left[-2\left(\theta_7^2+\theta_8^2\right)\right][\sigma_1^+\,\exp(2\,\theta_7\,a^\dagger)\exp(-2\,\theta_7\,a)\exp(2\,\theta_8\,b^\dagger)\exp(-2\,\theta_8\,b) + \sigma_1^-\,\exp(-2\,\theta_7\,a^\dagger)\exp(2\,\theta_7\,a)\exp(-2\,\theta_8\,b^\dagger)\exp(2\,\theta_8\,b)], \tag{54}$$

where $\mathcal{H}'$ is given by Eq. (52), θ_7 is the Lamb-Dicke parameter between qubit 1 and its nearest-neighbor resonator, and θ_8 is the Lamb-Dicke parameter between qubit 1 and its next-nearest-neighbor resonator (see Appendix B). Similarly to the case of a single qubit coupled to a single resonator, these two parameters are essential, as they allow us to quantify the nonlinearity of the Jaynes-Cummings model. The above time-dependent Hamiltonian is exempt from the cross-resonance term encountered in the Z*pq*Z case, which hindered scalable single-qubit manipulations (see Ref. [59] for a description of the Z*pq*Z case): this configuration, wherein each pair of neighboring physical qubits is coupled by means of two resonators via orthogonal degrees of freedom, allows us to circumvent this issue. We will not elaborate here on the calculation of the resulting effective Hamiltonian after switching to the rotating frame of the qubits and the resonators, as the justification of the RWA deserves further consideration. This point will be minutely examined in the next section. Here, we simply give expressions for the matrix elements associated with single-qubit manipulation and sideband transitions at any order with either the nearest-neighbor (NN) resonator [i.e., $\omega = |\Delta_1 - k_\alpha\,\omega_+|/\hbar$ and $\omega = (\Delta_1 + k_\alpha\,\omega_+)/\hbar$ for red and blue sideband transitions, respectively] and the next-nearest-neighbor (NNN) resonator [i.e., $\omega = |\Delta_1 - k_\beta\,\omega_-|/\hbar$ and $\omega = (\Delta_1 + k_\beta\,\omega_-)/\hbar$ for red and blue sideband transitions, respectively], assuming that the conditions of applicability of the RWA are fulfilled:

$$\langle\downarrow_1(n_\alpha+k_\alpha)n_\beta\psi_2|\mathcal{H}^{\rm RWA}_{\rm NN,red}|\uparrow_1 n_\alpha n_\beta\psi_2\rangle = (-1)^{k_\alpha}\langle\uparrow_1(n_\alpha+k_\alpha)n_\beta\psi_2|\mathcal{H}^{\rm RWA}_{\rm NN,blue}|\downarrow_1 n_\alpha n_\beta\psi_2\rangle = \frac{\Omega}{2}\,\exp\left[-2\left(\theta_7^2+\theta_8^2\right)\right](-2\,\theta_7)^{k_\alpha}\sqrt{\frac{n_\alpha!}{(n_\alpha+k_\alpha)!}}\,\mathrm{L}_{n_\alpha}^{k_\alpha}\left(4\,\theta_7^2\right)\mathrm{L}_{n_\beta}\left(4\,\theta_8^2\right), \tag{55}$$

$$\langle\downarrow_1 n_\alpha(n_\beta+k_\beta)\psi_2|\mathcal{H}^{\rm RWA}_{\rm NNN,red}|\uparrow_1 n_\alpha n_\beta\psi_2\rangle = (-1)^{k_\beta}\langle\uparrow_1 n_\alpha(n_\beta+k_\beta)\psi_2|\mathcal{H}^{\rm RWA}_{\rm NNN,blue}|\downarrow_1 n_\alpha n_\beta\psi_2\rangle = \frac{\Omega}{2}\,\exp\left[-2\left(\theta_7^2+\theta_8^2\right)\right](-2\,\theta_8)^{k_\beta}\sqrt{\frac{n_\beta!}{(n_\beta+k_\beta)!}}\,\mathrm{L}_{n_\alpha}\left(4\,\theta_7^2\right)\mathrm{L}_{n_\beta}^{k_\beta}\left(4\,\theta_8^2\right), \tag{56}$$

where $|\psi_2\rangle$ is an arbitrary state of qubit 2, $\mathrm{L}_n(x)$ is a Laguerre polynomial of degree n, and $\mathrm{L}_n^k(x)$ is an associated Laguerre polynomial.

In Fig. 9, we plot the matrix elements for single-photon sideband transitions between qubit 1 and either its nearest-neighbor or next-nearest-neighbor resonator [see Eqs. (55) and (56), with $k_\alpha = 1$ and $k_\beta = 1$ respectively]: these values are particularly interesting, as this type of sideband transition is needed in the mechanism (that we will describe later) to implement a controlled-phase gate. As might be expected, sideband transitions with the next-nearest-neighbor resonator are strongly dependent on the value of the fixed coupling g_c between both resonators, as can be seen in Fig 9(b).

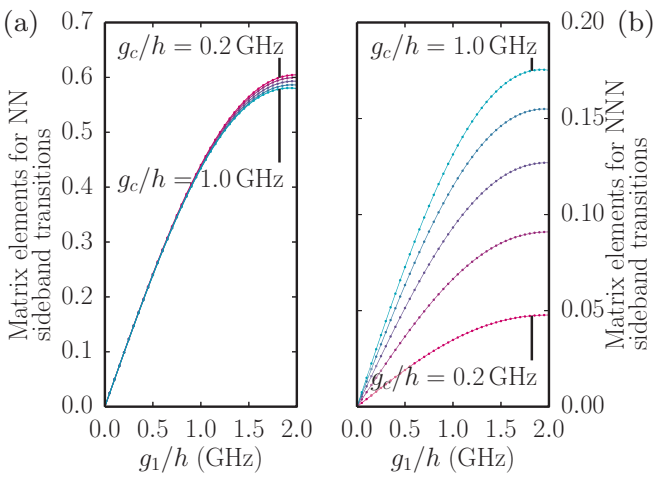

FIG. 9. (Color online) (a) Matrix elements for single-photon sideband transitions between qubit 1 and its nearest-neighbor (NN) resonator vs the coupling strength g_1, for different values of the coupling g_c between both resonators: their values for red sideband (i.e., $|\langle\downarrow_1 1_\alpha 0_\beta\psi_2|\sigma_1^x|\uparrow_1 0_\alpha 0_\beta\psi_2\rangle|$) and blue sideband (i.e., $|\langle\uparrow_1 1_\alpha 0_\beta\psi_2|\sigma_1^x|\downarrow_1 0_\alpha 0_\beta\psi_2\rangle|$) are identical. (b) The same is shown for sideband transitions between qubit 1 and its next-nearest-neighbor (NNN) resonator (either red or blue sideband, i.e., $|\langle\downarrow_1 0_\alpha 1_\beta\psi_2|\sigma_1^x|\uparrow_1 0_\alpha 0_\beta\psi_2\rangle|$ and $|\langle\uparrow_1 0_\alpha 1_\beta\psi_2|\sigma_1^x|\downarrow_1 0_\alpha 0_\beta\psi_2\rangle|$, respectively). In both cases, results obtained from numerical diagonalization (dots) are compared with the exact analytic formula (lines) ($\omega_1/h =$ 4 GHz, $\omega_2/h = 6$ GHz, and g_c/h ranges from 0.2 to 1 GHz in steps of 0.2 GHz). The values of Δ_1, Δ_2, and g_2 are irrelevant, and $|\psi_2\rangle$ is an arbitrary state of qubit 2. For numerical diagonalizations, the resonator Hilbert space is truncated to $n = 20$ Fock states.

3. *The holistic picture: discussion on the validity of the rotating wave approximation*

An important aspect of coupling physical qubits via their longitudinal degree of freedom is that once the residual interactions are compensated for at the level of a pair of neighboring qubits isolated from the rest of the register, this compensation will remain true within a 2D array. However, in the case where a transverse microwave drive is applied to one of the qubits—either to realize single-qubit operations or sideband transitions—the justification of the RWA can be hindered by the presence of the Bloch-Siegert oscillations. For an isolated qubit, this contribution to the time-dependent Hamiltonian is easily averaged out as long as the Rabi frequency Ω is small when compared with the resonant frequency Δ. Inside a 2D array like the one we are considering, however, this term may induce spurious

entanglement between each physical qubit and its surrounding resonators via unwanted higher-order sideband transitions [see Fig. 8(b)]. Similar issues hamper the speed of quantum gates in the case of trapped ions: the ac-Stark shifts caused by the presence of energy levels other than the one used to encode the information require us to find a trade-off between the speed at which the quantum register can be manipulated and the targeted accuracy [97]; otherwise, such shifts can be compensated for [98]. In what follows, we will assume that the resonators are all in their ground states: this allows us to consider a restricted number of higher order parametric processes (only those that involve the creation of photons simultaneously in one or more resonators while de-exciting the qubit), and ignore effects related to the nonlinearity of the Jaynes-Cummings model (i.e., the photon state dependence of the effective Rabi frequency).

The time-dependent Hamiltonian of the physical qubit p_0 driven by a transverse microwave drive is written as follows:

$$\mathcal{H}(t) = \mathcal{H} + \Omega(t)\cos(\omega t + \phi)\sigma^x_{p_0}, \tag{57}$$

where Ω, ω, and ϕ are the amplitude, the frequency, and the phase of the microwave drive, respectively.

We apply the same set of unitary transformations to diagonalize the fixed interactions related to the eight resonators and the four qubits surrounding the qubit p_0 following the method described in Appendix B, so that the previous time-dependent Hamiltonian becomes

$$\begin{aligned}\mathcal{H}'(t) = \mathcal{H}' + \Omega(t)\cos(\omega t + \phi)\exp\left[-2\sum_{i\in\{\uparrow,\rightarrow,\downarrow,\leftarrow\}}\left(\theta_{7i}^2 + \theta_{8i}^2\right)\right]\\ \times\left[\sigma^+_{p_0}\prod_{j\in\{\uparrow,\rightarrow,\downarrow,\leftarrow\}}\exp(2\,\theta_{7j}\,a_j^\dagger)\exp(-2\,\theta_{7j}\,a_j)\exp(2\,\theta_{8j}\,b_j^\dagger)\exp(-2\,\theta_{8j}\,b_j)\right.\\ \left.+\,\sigma^-_{p_0}\prod_{j\in\{\uparrow,\rightarrow,\downarrow,\leftarrow\}}\exp(-2\,\theta_{7j}\,a_j^\dagger)\exp(2\,\theta_{7j}\,a_j)\exp(-2\,\theta_{8j}\,b_j^\dagger)\exp(2\,\theta_{8j}\,b_j)\right].\end{aligned} \tag{58}$$

In order to switch to the rotating frame of the physical qubit p_0 and the eight neighboring resonators, we apply the following time-dependent unitary transformation:

$$\mathcal{U} = \exp\left[-\mathrm{i}\frac{(\Delta_{p_0}t + \phi_{p_0})}{2}\sigma^z_{p_0}\right]\prod_{i\in\{\uparrow,\rightarrow,\downarrow,\leftarrow\}}\exp[-\mathrm{i}(\omega_i^+ t + \phi_i^+)a_i^\dagger a_i - \mathrm{i}(\omega_i^- t + \phi_i^-)b_i^\dagger b_i]. \tag{59}$$

The resulting time-dependent Hamiltonian thus reads

$$\begin{aligned}\mathcal{H}''(t) = \Omega(t)\cos(\omega t + \phi)\exp\left[-2\sum_{i\in\{\uparrow,\rightarrow,\downarrow,\leftarrow\}}\left(\theta_{7i}^2 + \theta_{8i}^2\right)\right]\\ \times\left\{\mathrm{e}^{\mathrm{i}(\Delta_{p_0}t+\phi_{p_0})}\sigma^+_{p_0}\prod_{j\in\{\uparrow,\rightarrow,\downarrow,\leftarrow\}}\exp[2\,\theta_{7j}\,\mathrm{e}^{\mathrm{i}(\omega_j^+t+\phi_j^+)}a_j^\dagger]\exp[-2\,\theta_{7j}\,\mathrm{e}^{-\mathrm{i}(\omega_j^+t+\phi_j^+)}a_j]\right.\\ \times\exp[2\,\theta_{8j}\,\mathrm{e}^{\mathrm{i}(\omega_j^-t+\phi_j^-)}b_j^\dagger]\exp[-2\,\theta_{8j}\,\mathrm{e}^{-\mathrm{i}(\omega_j^-t+\phi_j^-)}b_j]\\ +\mathrm{e}^{-\mathrm{i}(\Delta_{p_0}t+\phi_{p_0})}\sigma^-_{p_0}\prod_{j\in\{\uparrow,\rightarrow,\downarrow,\leftarrow\}}\exp[-2\,\theta_{7j}\,\mathrm{e}^{\mathrm{i}(\omega_j^+t+\phi_j^+)}a_j^\dagger]\exp[2\,\theta_{7j}\,\mathrm{e}^{-\mathrm{i}(\omega_j^+t+\phi_j^+)}a_j]\\ \left.\times\exp[-2\,\theta_{8j}\,\mathrm{e}^{\mathrm{i}(\omega_j^-t+\phi_j^-)}b_j^\dagger]\exp[2\,\theta_{8j}\,\mathrm{e}^{-\mathrm{i}(\omega_j^-t+\phi_j^-)}b_j]\right\}.\end{aligned} \tag{60}$$

The Debye-Waller factor $\mathcal{D}$ is now defined as

$$\mathcal{D} = \exp\left[-2\sum_{i\in\{\uparrow,\rightarrow,\downarrow,\leftarrow\}}\left(\theta_{7i}^2 + \theta_{8i}^2\right)\right]. \tag{61}$$

Let us consider the case of single-qubit operations. Thus, we set $\omega = \Delta_{p_0}/\hbar$, and all phases equal to zero for the sake of simplicity. First-order sideband transitions with one α or one β resonator (left) are averaged out provided that the following conditions of applicability of the RWA (right) are well justified:

$$\begin{aligned}\left(\sigma^+_{p_0}a_i + \sigma^-_{p_0}a_i^\dagger\right) &\Rightarrow \mathcal{D}\,\theta_{7i}\,\Omega \ll \left|2\,\Delta_{p_0} - \omega_i^+\right|\\ \left(\sigma^+_{p_0}b_i + \sigma^-_{p_0}b_i^\dagger\right) &\Rightarrow \mathcal{D}\,\theta_{8i}\,\Omega \ll \left|2\,\Delta_{p_0} - \omega_i^-\right|.\end{aligned} \tag{62}$$

Similarly, second-order sideband transitions with two α, two β, or with one α and one β resonators (left) are averaged out provided that the conditions of applicability of the RWA

(right) are well justified:

$$\left(\sigma_{p_0}^{+} a_i a_j + \sigma_{p_0}^{-} a_i^{\dagger} a_j^{\dagger}\right) \Rightarrow 2\mathcal{D}\theta_{7i}\,\theta_{7j}\Omega \ll \left|2\Delta_{p_0} - (\omega_i^{+} + \omega_j^{+})\right|$$

$$\left(\sigma_{p_0}^{+} b_i b_j + \sigma_{p_0}^{-} b_i^{\dagger} b_j^{\dagger}\right) \Rightarrow 2\mathcal{D}\theta_{8i}\,\theta_{8j}\Omega \ll \left|2\Delta_{p_0} - (\omega_i^{-} + \omega_j^{-})\right|$$

$$\left(\sigma_{p_0}^{+} a_i b_j + \sigma_{p_0}^{-} a_i^{\dagger} b_j^{\dagger}\right) \Rightarrow 2\mathcal{D}\theta_{7i}\,\theta_{8j}\Omega \ll \left|2\Delta_{p_0} - (\omega_i^{+} + \omega_j^{-})\right|. \tag{63}$$

We assume that higher-order sideband transitions will be averaged out because the prefactor, which is a product of θ_{7i} and θ_{8j}, becomes increasingly small, and the conditions on the detuning become less stringent. If the previous conditions are well justified, and if all the resonators are in their ground states, the matrix elements associated with single-qubit operations are given by

$$\langle 0,\uparrow|\,\mathcal{H}_{\mathrm{sq}}^{\mathrm{RWA}}\,|0,\downarrow\rangle = \frac{\Omega}{2}\,\mathcal{D}, \tag{64}$$

where $\mathcal{D}$ is the Debye-Waller factor comprising the effect of the eight surrounding resonators [see Eq. (61)]. The notation $|0\rangle$ in the above expression implies that all resonators are in their ground states. The justification of the RWA is made more difficult by the presence of the Bloch-Siegert oscillations: this problem can be a serious limitation on the fidelity of single-qubit and two-qubit operations if the parameters are not properly adjusted. Ensuring the validity of the RWA also has a practical implication. It is preferable to use single-mode resonators (lumped element resonators) to mediate the interactions between qubits, as the presence of higher-modes in multimode resonators (1D cavities) would require more conditions to be met in order to neglect unwanted sidebands.

4. Implementation of a controlled phase gate

In their seminal work, Cirac and Zoller showed how sideband transitions could be used to realize a CNOT gate in the context of quantum computation with trapped ions [37]. Their proposal requires an extra atomic degree of freedom, which in our case may not be a suitable option as it would complicate the justification of the RWA. Schematically, the idea sustaining this type of approach is to transfer the state of the target qubit into a photon state via a red sideband transition (half-period), apply a second red sideband transition (one period) that is associated with the third level of the control qubit and the resonator and that couples only to the state which is initially $|\downarrow_1\uparrow_2\rangle$ (thus selectively inducing a global phase accumulation π), and transfer the photon state back into the target qubit state via another red sideband transition (half-period). This pulse sequence generates a controlled-phase gate, which allows us to define a CNOT gate if it is supplemented by two Hadamard gates applied to the target qubit. This idea was first implemented by Monroe *et al.* between two states related to the same trapped ion [38]; one encoded in its hyperfine states and the other encoded in its quantized harmonic motion.

Ideally, one may want to realize a similar process of conditional phase accumulation without resorting to an auxiliary level of the ion. The difficulty in this type of approach is the dependence of the matrix elements for sideband transitions on the photon state of the resonator, even in the Lamb-Dicke regime. Monroe *et al.* suggested the operation of such a system outside of the Lamb-Dicke regime, and to adjust the Rabi frequencies of the internal state of the ion depending on the state of the harmonic oscillator by choosing the Lamb-Dicke parameter η in such a way that after a laser pulse, the state of the ion returns to its initial state if $|n\rangle = |0\rangle$ or flipped if $|n\rangle = |1\rangle$, thus defining a CNOT gate [99]. However, this idea cannot be applied in our case, i.e., a 2D array of physical qubits: the proper conditions on the Lamb-Dicke parameter η cannot be fulfilled simultaneously for each physical qubit and its four nearest-neighbor resonators. An alternate solution inspired by NMR is to use a composite pulse sequence which preserves the computational subspace [39,100]. This method is valid in the Lamb-Dicke regime, and it is consequently not suitable for our purpose, as we wish to keep the benefit of being able to operate our system with a large atom-photon interaction strength g (i.e., arbitrary $\eta = 2\,g/\omega_r$).

In order to overcome the aforementioned limitation, one possibility in our layout is to use the fact that we have two resonators in between each pair of nearest-neighboring qubits in the array: the idea is to use an already existing extra degree of freedom among the resonators, instead of introducing an extra atomic degree of freedom by playing with the anharmonicity of our artificial atoms. Basically, our goal is to encode one of the qubit states $\{|\downarrow\rangle, |\uparrow\rangle\}$ into a two-mode state $\{|00\rangle, |01\rangle\}$, which can be manipulated via a beam-splitter $(a^{\dagger}b + ab^{\dagger})$. The underlying motivation for this choice is the SU(2) Lie algebraic structure of the beam-splitter operation, which intrinsically prevents any leakage of information out of the computational subspace, a well-known property of quantum optics. This encoding allows us to overcome the nonlinearity of the Jaynes-Cummings model without reducing the anharmonicity of the flux qubits, thus preventing the risk of leakage while performing single-qubit operations and simplifying the justification of the RWA, as was originally intended.

Let us consider an arbitrary initial state $|\psi\rangle$, assuming that both neighboring resonators are in their ground states:

$$\begin{aligned}|\psi\rangle = {} & \alpha\,|\downarrow_1 0_\alpha 0_\beta \downarrow_2\rangle + \beta\,|\downarrow_1 0_\alpha 0_\beta \uparrow_2\rangle \\ & + \gamma|\uparrow_1 0_\alpha 0_\beta \downarrow_2\rangle + \delta|\uparrow_1 0_\alpha 0_\beta \uparrow_2\rangle.\end{aligned} \tag{65}$$

Then, we map the state of qubit 2 onto the resonators state by applying a red sideband transition between resonator β and qubit 2 for a half-period $(b^{\dagger}\sigma_2^{-} + b\sigma_2^{+})$. The ground state of qubit 2 is thus encoded as $|0_\alpha 0_\beta\rangle$, whereas its excited state is encoded as $|0_\alpha 1_\beta\rangle$. The state resulting from this operation reads

$$\begin{aligned}|\psi\rangle = {} & \alpha|\downarrow_1 0_\alpha 0_\beta \downarrow_2\rangle + \mathrm{i}\,\beta|\downarrow_1 0_\alpha 1_\beta \downarrow_2\rangle \\ & + \gamma|\uparrow_1 0_\alpha 0_\beta \downarrow_2\rangle + \mathrm{i}\,\delta|\uparrow_1 0_\alpha 1_\beta \downarrow_2\rangle.\end{aligned} \tag{66}$$

Subsequently, we must apply the sideband transition $(\sigma_1^{+}a^{\dagger}b + \sigma_1^{-}ab^{\dagger})$ for one period. This transition is exclusively coupled to the state $|\downarrow_1 0_\alpha 1_\beta \downarrow_2\rangle$, which allows a selective accumulation of global phase π for this state only. Hence the ensuing state is

$$\begin{aligned}|\psi\rangle = {} & \alpha|\downarrow_1 0_\alpha 0_\beta \downarrow_2\rangle - \mathrm{i}\,\beta|\downarrow_1 0_\alpha 1_\beta \downarrow_2\rangle \\ & + \gamma|\uparrow_1 0_\alpha 0_\beta \downarrow_2\rangle + \mathrm{i}\,\delta|\uparrow_1 0_\alpha 1_\beta \downarrow_2\rangle.\end{aligned} \tag{67}$$

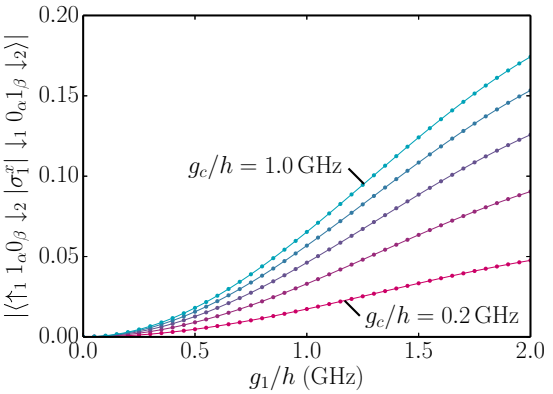

FIG. 10. (Color online) Matrix element for the sideband transition ($\sigma_1^+ a^\dagger b + \sigma_1^- a b^\dagger$) used in the conditional-phase accumulation mechanism ($\omega_1/h = 4$ GHz, $\omega_2/h = 6$ GHz, and g_c/h ranges from 0.2 to 1 GHz in steps of 0.2 GHz, the values of Δ_1, Δ_2, and g_2 are irrelevant). Results obtained from numerical diagonalization (dots) are compared with the exact analytic formula (lines). For numerical diagonalizations, the resonator Hilbert space is truncated to $n = 20$ Fock states.

Eventually, we map the resonators state back onto the state of qubit 2 by applying a red sideband transition between resonator β and qubit 2 for a half-period ($b^\dagger\sigma_2^- + b\sigma_2^+$). The final state we obtain is given by

$$|\psi\rangle = \alpha|\downarrow_1 0_\alpha 0_\beta \downarrow_2\rangle + \beta|\downarrow_1 0_\alpha 0_\beta \uparrow_2\rangle + \gamma|\uparrow_1 0_\alpha 0_\beta \downarrow_2\rangle - \delta|\uparrow_1 0_\alpha 0_\beta \uparrow_2\rangle. \quad (68)$$

The above pulse sequence effectively realizes a controlled-phase gate on the two-qubit state, which, complemented by the usual microwave-induced single-qubit gates, allows us to define *a "universal" set of quantum gates*. The sideband transition ($\sigma_1^+ a^\dagger b + \sigma_1^- a b^\dagger$) can be induced by driving qubit 1 at the frequency $|\Delta_1 + \omega_+ - \omega_-|/h$. The matrix element associated with this transition reads

$$\langle\uparrow_1 1_\alpha 0_\beta \downarrow_2|\mathcal{H}^{\mathrm{RWA}}|\downarrow_1 0_\alpha 1_\beta \downarrow_2\rangle = -\frac{\Omega}{2}\mathcal{D}(4\theta_7\theta_8), \quad (69)$$

where θ_7 and θ_8 are the aforementioned Lamb-Dicke parameters (see Appendix B), and the Debye-Waller factor $\mathcal{D}$ is given by $\exp[-2(\theta_7^2 + \theta_8^2)]$. For the sake of completeness, we compare the value of these matrix elements based on this analytic expression with the result given by a numerical diagonalization [see Fig. 10]. We find a good agreement, as is expected considering that the simplicity of the interactions involved in this coupling scheme allows an exact theoretical treatment. The coupling strengths between the qubit and the nearest-neighbor resonator, and between both resonators (i.e., respectively g_1 and g_c) have a comparable influence on the strength of this tunable interaction. Accordingly, it is quite favorable to operate this system in the limit of large g_c, whereas the single-mode sideband transitions involved in the first and the last step of this two-qubit gate are quite insensitive to it [see Figs. 9(a) and 9(b)]. Similar to the Cirac and Zoller scheme, implementing a controlled-phase gate in this way does not require the adjustment of the phase of the microwave signals involved in the mechanism of conditional accumulation of global phase relative to the reference phases of the rotating frame of each qubit.

As mentioned earlier, this scheme requires us to operate the system in the low temperature limit, in order to suppress the thermal population of the resonators. Thermal excitation of higher photon states of the resonators, combined with the photon state dependence of the effective Rabi frequency of sideband transitions, would generate spurious entanglement between qubits and resonators.

5. Readout

Evidently, the absence of dispersive shift impedes the determination of the qubit state via dispersive measurement. Actually, the dispersive shift solely represents the contribution to the resonator dynamics inherited from the static Hamiltonian, but there could be a useful term in the time-dependent part. We verify that this is not the case (see Ref. [59] for details). Here, we draw inspiration from the analogy with ion traps to circumvent the aforesaid issue. The idea of electron shelving introduced by Dehmelt is a process of quantum amplification based on an asymmetric double resonance [101]. The resonance fluorescence associated with the strong transition allows us to detect the quantum state associated with the weak one. Ion-trap systems greatly benefit from this method for detection of quantum states on account of its high efficiency. Its implementation at an early stage allowed the first observation of quantum jumps [102–104]. More recently, Myerson *et al.* demonstrated single-shot qubit readout with a fidelity as high as 99.99% [105], thus meeting the constraints imposed by quantum error correction.

Englert *et al.* proposed an extension of this idea in the context of XcQED [106]. They considered a three-level system in which the information was encoded in the ground state and the first excited state, coupled transversely to a quantum harmonic oscillator. It was required that the resonator frequency ω_r be equal to the energy difference between the first and second excited states of the atom ω_{eu}. By resonantly driving the transition between the first and second excited states ($|e\rangle \leftrightarrow |u\rangle$) of the artificial atom at the frequency $\omega_d = \omega_r = \omega_{eu}$, one could generate a conditional displacement of the field in the resonator, which was proportional to the population of the atom in its first excited state $|e\rangle$. Measuring the number of photons in the resonator gave direct access to the state of the qubit, which was encoded in the ground and the first excited states.

Our first approach consists of transposing the proposal of Englert *et al.* [106] to ZcQED: let us assume that we operate a three-level atom longitudinally coupled to a resonator. A flux qubit with a reduced anharmonicity and operated at its symmetry point is a three-level ladder system (Ξ). This selection rule offers an extra atomic degree of freedom without excessively complicating the justification of the RWA for single-qubit operations and sideband transitions. The idea is to simultaneously apply a set of red and blue sideband transitions associated with the transition from the first excited state to the second excited state of the atom and either a nearest-neighbor or a next-nearest-neighbor resonator, as depicted in Fig. 11, assuming that the resonator is initially in its ground state. The photon state of the resonator remains unchanged if the qubit is

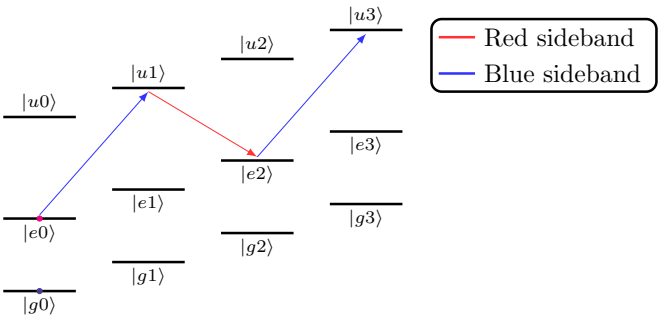

FIG. 11. (Color online) Energy level diagram representing the effect of combined red and blue sideband transitions associated with the transition from the first excited state to the second excited state in the case of a three-level atom, for an arbitrary initial state of the qubit.

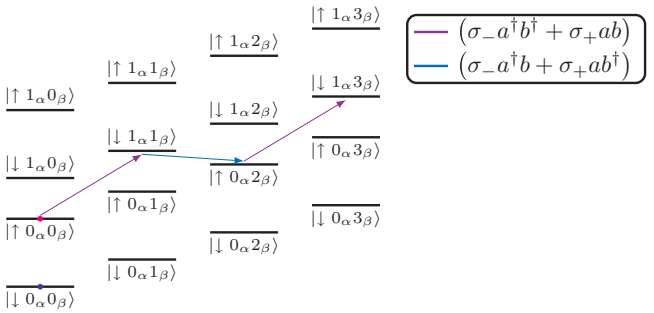

FIG. 12. (Color online) Energy level diagram representing the effect of combined single-qubit and two-resonator sideband transitions in the case of a two-level atom, for an arbitrary initial state of the qubit.

initially in its ground state, whereas if it is in its excited state, it will evolve with time by climbing the Jaynes-Cummings ladder.

This scheme is more flexible in ZcQED because it does not require strict conditions on the atom and resonator energy scales, as in the proposal of Englert *et al.* The absence of dispersive shift offered by the longitudinal coupling to the atomic degrees of freedom guarantees that these sideband transitions remain resonant, independent of the photon state of the resonator, thus allowing to climb the Jaynes-Cummings ladder. In the case of XcQED, since the matrix elements associated with these sideband transitions are independent of the photon state of the resonator, the number of photons rises in proportion to the amount of time over which the readout pulse is applied [106]. In ZcQED, however, the nonlinearity of the Jaynes-Cummings model does not allow for a straightforward relationship between the length of the readout pulse and the number of photons in the resonator. This type of effect will be illustrated subsequently.

This readout scheme applies to artificial atoms with a weak anharmonicity (namely phase qubits, transmons and Xmons). We will not detail this approach any further, as we wish to avoid the introduction of a third level to the atom, as already mentioned earlier; our aim was to show how XcQED and ZcQED compare to each other in this specific example. We consider another method that does not require the presence of a third level, and can be operated with one resonator by combining single- and two-photon sideband transitions; though this approach is not suitable for our purposes owing to its poor readout efficiency, it illustrates the difficulty of applying electron shelving techniques to our layout without adding an extra degree of freedom (see Ref. [59] for details).

The final readout scheme we consider relies on the combination of two single-qubit and two-resonator sideband transitions: either $(\sigma_- a^\dagger b^\dagger + \sigma_+ ab)$ and $(\sigma_- ab^\dagger + \sigma_+ a^\dagger b)$, or $(\sigma_- a^\dagger b^\dagger + \sigma_+ ab)$ and $(\sigma_- a^\dagger b + \sigma_+ ab^\dagger)$. The first combination fills the nearest-neighbor resonator, whereas the second one fills the next-nearest-neighbor resonator, as depicted in Fig. 12. It is this latter option that we will retain, as it is less sensitive to the nonlinearity of the Jaynes-Cummings model for the reason given below. The main merit of this scheme is that the matrix elements associated with these two sidebands have the same associated Laguerre polynomial dependence. Consequently, these two processes cooperate well, thus ensuring that the next-nearest-neighbor resonator will be filled with a significant number of photons and potentially allowing a single-shot readout.

In order to illustrate the role of the nonlinearity of the Jaynes-Cummings model on the readout efficiency, we perform some numerical simulations to compare both approaches. The interaction Hamiltonian is treated within the RWA, and the amplitudes of the microwave drive for both sideband transitions are taken to be equal. In the case where we fill the nearest-neighbor resonator, the matrix elements for the sideband transitions $(\sigma_- a^\dagger b^\dagger + \sigma_+ ab)$ and $(\sigma_- ab^\dagger + \sigma_+ a^\dagger b)$ are given by

$$\begin{aligned}&\langle\downarrow(n_\alpha+1)1_\beta|\mathcal{H}^{\mathrm{RWA}}|\uparrow n_\alpha 0_\beta\rangle\\&\quad=-\langle\downarrow n_\alpha 1_\beta|\mathcal{H}^{\mathrm{RWA}}|\uparrow(n_\alpha+1)0_\beta\rangle\\&\quad=-\frac{\Omega}{2}\exp\left[-2\left(\theta_7^2+\theta_8^2\right)\right]\frac{4\theta_7\theta_8}{\sqrt{n_\alpha+1}}\,\mathrm{L}^1_{n_\alpha}\left(4\theta_7^2\right),\end{aligned}\tag{70}$$

whereas in the case where we fill the next-nearest-neighbor resonator, the matrix elements for the sideband transitions $(\sigma_- a^\dagger b^\dagger + \sigma_+ ab)$ and $(\sigma_- a^\dagger b + \sigma_+ ab^\dagger)$ read

$$\begin{aligned}&\langle\downarrow 1_\alpha(n_\beta+1)|\mathcal{H}^{\mathrm{RWA}}|\uparrow 0_\alpha n_\beta\rangle\\&\quad=-\langle\downarrow 1_\alpha n_\beta|\mathcal{H}^{\mathrm{RWA}}|\uparrow 0_\alpha(n_\beta+1)\rangle\\&\quad=-\frac{\Omega}{2}\exp\left[-2\left(\theta_7^2+\theta_8^2\right)\right]\frac{4\theta_7\theta_8}{\sqrt{n_\beta+1}}\,\mathrm{L}^1_{n_\beta}\left(4\theta_8^2\right),\end{aligned}\tag{71}$$

where $\mathrm{L}^1_n(x)$ stands for the associated Laguerre polynomial of degree n.

The associated Laguerre polynomial L^1_n dependence of these matrix elements as a function of the Lamb-Dicke parameter is responsible for their cancellation for some particular Fock state; this cancellation occurs for higher Fock states when we fill the next-nearest-neighbor resonator, rather than when we fill the nearest-neighbor resonator [see Figs. 13(a) and 13(c)], simply because the Lamb-Dicke parameter for the mediated interaction θ_8 is smaller than the one for the direct interaction θ_7. Consequently, when climbing the Jaynes-Cummings ladder with the bichromatic microwave drive applied for readout, the

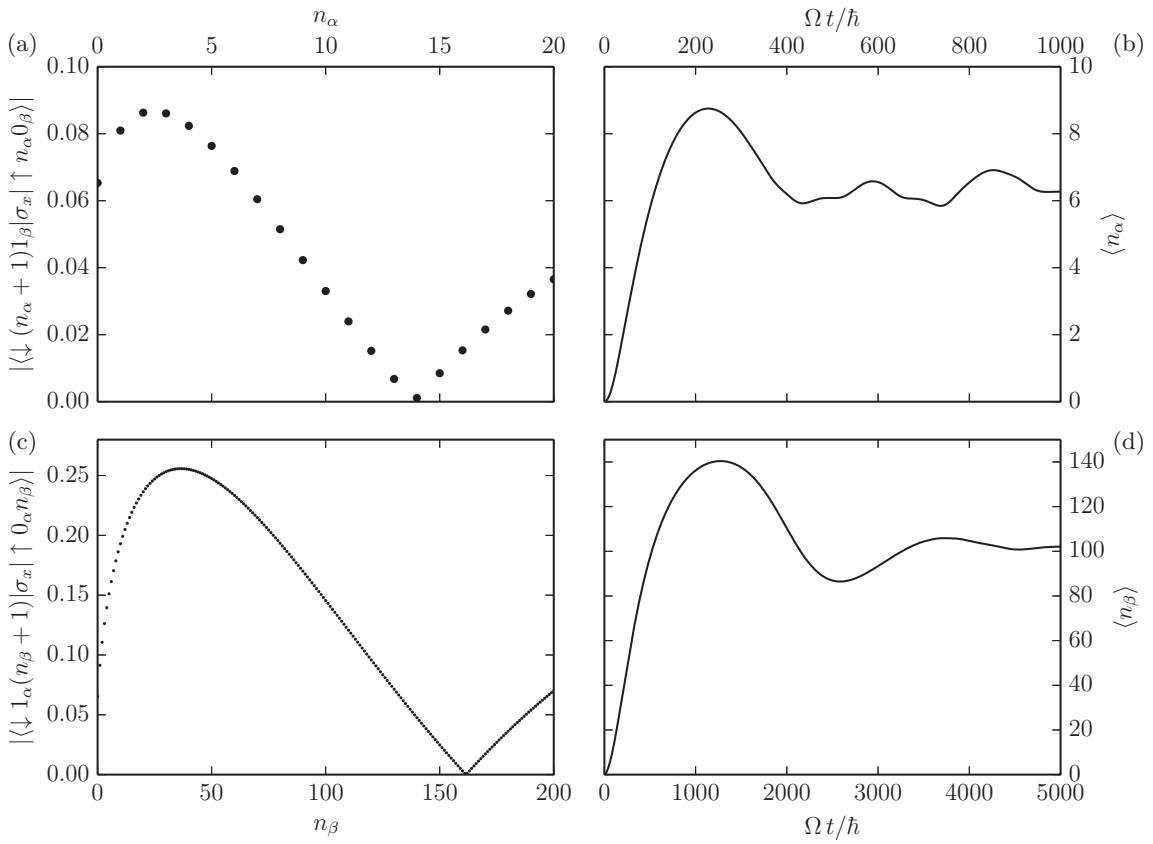

FIG. 13. The dependence of the matrix elements associated with the sideband transitions involved in the readout process vs the Fock state of (a) the nearest-neighbor resonator, and (c) the next-nearest-neighbor resonator. The intracavity mean photon number vs the length of the bichromatic microwave pulse applied for readout in the case where we fill (b) the nearest-neighbor resonator, and (d) the next-nearest-neighbor resonator. The considered parameters of the device are $\omega_1/h = 4$ GHz, $\omega_2/h = 6$ GHz, $g_1/h = 1$ GHz, and $g_c/h = 1$ GHz, while the value of g_2 is irrelevant.

mean photon number in the readout resonator saturates for larger values when we fill the next-nearest-neighbor resonator than it does when we fill the nearest-neighbor resonator [see Figs. 13(b) and 13(d)], thus offering a higher readout efficiency for the same amplitude of the applied microwave drive. For the sake of completeness, we also determine the time-evolution of the photon number distribution in the readout resonator in both configurations (see animations in Ref. [59]).

The question arises of how to detect these photons afterward. The circuit should be designed in such a way that half of the resonators are coupled to transmission lines that convey photons to microwave amplifiers—let us say that the α resonators are uncoupled and the β resonators are coupled, for example [see Fig. 8(a)]. If the coupling is fixed, then all of the β resonators will have a low quality factor which would tend to reduce the fidelity of the controlled-phase gate we described previously, as it relies on a two-mode sideband transition. To avoid this issue, it may be preferable to use a tunable coupler based on variable inductance, as demonstrated by Yin *et al.* [107], for example. It could be argued that in principle, this type of device is sufficient for implementing tunable interactions between qubits with a very high ON/OFF ratio [108]. The choice of a circuit QED based architecture is motivated by two advantages: the ease of controlling the distance between qubits, which allows us to suppress cross-talk, and the possibility of integrating the circuits used to mediate the interactions and to read out the state of the qubits in the same layout.

Another positive aspect that must be mentioned about this readout scheme is its quantum nondemolition-like (QND-like) nature. Strictly speaking, this readout process is not QND, as the applied sideband transitions do not commute with the free Hamiltonian of the qubit. Nevertheless, the qubit excitation remains encoded in a superposition of states involving the qubit and the witness resonator. If we consider the case where we use the next-nearest-neighbor resonator for readout, then the initial excitation of the qubit will be retained as a superposition of the states $|\uparrow 0_\alpha\rangle$ and $|\downarrow 1_\alpha\rangle$, where $|0_\alpha\rangle$ and $|1_\alpha\rangle$ are the Fock states of the nearest-neighbor resonator, as depicted in Fig. 12. This means that after applying the readout pulse, the initial state of the qubit can be restored by applying a red sideband transition $(\sigma_- a^\dagger + \sigma_+ a)$, thus guaranteeing the QND-like nature of the readout.

This scheme also has the merit that the determination of the number of photons in the readout resonator does not significantly adversely affect the coherence properties of the qubit to be read out or of the witness qubit (say qubits 1 and 2, respectively with the present notation). As already detailed, one advantage inherent to ZcQED is that the qubit relaxation rate is unaffected by the photon lifetime of the resonator, regardless of the state of the latter (see Sec. III A 3).

This implies that when the coupling between the readout resonator and the transmission line is turned on, the state of the witness qubit will not be altered by its lowered quality factor. Nonetheless, the qubit relaxation rate is affected by the readout procedure via the photon state dependence of the matrix elements $\langle\downarrow_1,n_\alpha,n_\beta,\psi_2|\sigma_1^x|\uparrow_1,n_\alpha,n_\beta,\psi_2\rangle$. For a given photon state $|n_\alpha,n_\beta\rangle$ of the two resonators, the relaxation rate of qubit 1 reads as follows:

$$\Gamma_{\gamma_{q_1}}^{\{n_\alpha,n_\beta\}} = \gamma_{q_1}\, \exp\left[-4\left(\theta_7^2+\theta_8^2\right)\right]\left[L_{n_\alpha}\left(4\,\theta_7^2\right)\, L_{n_\beta}\left(4\,\theta_8^2\right)\right]^2, \tag{72}$$

where $1/\gamma_{q_1}$ is the lifetime of qubit 1 due to intrinsic decay processes of the bare qubit state, and $L_n(x)$ is a Laguerre polynomial of degree n.

The issue of correlated errors corresponding to the simultaneous relaxation of the qubit state and either relaxation or excitation of the two-mode states, which we already discussed in the case of a single bosonic mode (see Sec. III A 3), may have a more severe backaction. Ironically, these effects may be more pronounced for the witness qubit as we are filling the next-nearest-neighbor resonator. A way to circumvent this issue is to momentarily map the state of the witness qubit onto a two-mode state, $\{|00\rangle, |01\rangle\}$, of one of the three other pairs of resonators surrounding it via red sideband transitions during the readout. This implies that the state of the other qubit attached to this second pair of resonators should not be manipulated during that time. We also verify that the absence of the Purcell effect, which we previously highlighted in the case of one resonator (see Sec. III A 3), persists in this configuration: the effect of the photon lifetime of each bare resonator is converted into two independent single-photon errors, and it does not introduce correlated errors (see Ref. [59] for details).

Furthermore, in the case of dispersive readout used in XcQED, the presence of the dispersive shift renders the qubit dephasing sensitive to the quantum fluctuations associated with the photons populating the resonator when the readout pulse is applied (measurement-induced dephasing [109,110]). The layout we are considering being free of dispersive shift, this type of readout does not exert any backaction on the dephasing rate of the qubits surrounding the resonator used for the readout. Moreover, it fulfills the fifth DiVincenzo criterion, as it provides *a qubit-specific measurement capability*. The number of photons in the readout resonator is unequivocally related to the state of the qubit to be read out, and is not affected by the states of its neighbors, which is another advantage of coupling physical qubits via their longitudinal degree of freedom.

Here again, it is more suitable to work in the quantum limit: thermal excitations of the resonators would complicate the readout process, as it would involve a larger number of states in a rather nontrivial way. This also means that the resonators must be properly reset after each readout, so as to guarantee the fidelity of subsequent measurements and two-qubit operations.

6. *Initialization*

At last, we will briefly describe a simple way to reset the state of the qubits using red sideband transitions. As the effective Rabi frequency of the sideband transitions depends upon the photon state of the resonator, we must ensure that the one we use for qubit initialization is in its ground state in order to guarantee the fidelity of the quantum state transfer and the efficiency of the qubit initialization accordingly. For this reason, it is again essential to operate the system in the limit of low temperature. We thus consider using one of the resonators used for readout (say, a β resonator to keep the same notation as in Sec. III C 5). Furthermore, we assume that this resonator has been properly reset if it has been used for readout beforehand, by keeping the coupling with the transmission line on for long enough. The qubit is initially in an unknown state $|\psi\rangle = c_\downarrow|\downarrow 0_\beta\rangle + c_\uparrow|\uparrow 0_\beta\rangle$; if we apply a red sideband transition ($\sigma_- b^\dagger + \sigma_+ b$) over a half-period, the residual excitation of the qubit is transferred to the resonator and the system becomes $|\psi'\rangle = c_\downarrow|\downarrow 0_\beta\rangle + c_\uparrow|\downarrow 1_\beta\rangle$. After that, it remains to reset the state of the resonator.

IV. CONCLUSIONS

We reviewed several aspects of circuit QED in the customary configuration wherein an artificial atom is transversely coupled to a quantum harmonic oscillator (XcQED). We discussed how to capitalize on the possibility of *in situ* control of the longitudinal degree of freedom of superconducting qubits to circumvent the parity selection rule, either to realize sideband transitions in the manner of trapped ions, or to realize parametric conversion between two qubits. However, in this layout, sideband transitions are adversely affected by the rather large dispersive shifts and the photon lifetime in the resonator. Two-qubit parametric conversion has the merit of generating entanglement between physical qubits without creating real excitations in the resonator, and is a possible alternative to cross-resonance, which has the advantage of being more immune to cross-talk [64].

We introduced a new paradigm for circuit QED systems, where an artificial atom is coupled via its longitudinal degree of freedom to a quantum harmonic oscillator (ZcQED). This layout avoids the presence of nonlinearities (such as Kerr nonlinearity) and residual interactions between the qubit and the resonator (dispersive shift). Based on this idea, we described few different possibilities for mediating the interaction between two qubits. Our aim was to find a configuration wherein we would have concomitantly *well-characterized qubits* and *a "universal" set of quantum gates*. We found that the latter two requirements can be fulfilled if the interaction is mediated through two resonators fixedly coupled, each resonator being coupled separately to one of the two qubits and the other resonator via orthogonal degrees of freedom. This layout retains the advantage of having well-defined energy levels for qubits and resonators, as observed in the case of a single qubit longitudinally coupled to a single resonator (in the absence of dispersive shift, self-Kerr, and cross-Kerr nonlinearities, and residual $\sigma_z\sigma_z$ interactions), while allowing scalable single-qubit operations and sideband transitions. This coupling scheme has the merit of keeping the aforesaid properties once included in an array of arbitrary dimension and topology, as the free Hamiltonian of each physical qubit commutes with the coupling terms with the surrounding resonators. Such a unit cell can be integrated among a 2D

square lattice of qubits, which is the requisite architecture for fault-tolerant quantum computation based on the surface code.

We presented a way to realize a controlled-phase gate between both qubits comprised in such unit cell, based on sideband transitions in a similar manner to the proposal of Cirac and Zoller in the context of trapped ions [37]: we proposed to encode the state of one of the two qubits into a two-mode state of the resonators, and use a two-mode sideband transition to selectively accumulate a global phase π for one of the four two-qubit states, instead of using a three-level artificial atom as in the latter reference.

We described a readout scheme that allows a QND-like measurement of the qubit state conceived by analogy with the idea of electron shelving. It takes advantage of the fact that we have two resonators in between each pair of neighboring qubits in the 2D array instead of requiring an extra atomic degree of freedom, as in the proposal by Englert *et al.* in the context of XcQED [106], thus bringing no additional complication to the justification of the RWA. More importantly, we showed how to overcome the limitations imposed by the nonlinear Jaynes-Cummings model, bringing the possibility of achieving single-shot readout within reach.

A rather obvious objection to this latter approach is that coupling qubits via their longitudinal degree of freedom naturally increases their sensitivity to low-frequency noise; however, qubit dephasing can be efficiently mitigated using dynamical decoupling [111–117]. It is more favorable to manipulate the state of a system with well-defined energy levels and suppress the spurious accumulation of phase all along the computation by ensuring the exact cancellation of residual interactions, while preserving resources to counteract qubit dephasing with error suppression.

The coherence time enhancement of transmons observed in a 3D cavity showed that there is still room for improvement of these devices [45]. The architecture described in this work is more likely to be integrated in a planar layout: shielding from infrared radiation, improved circuit designs, and progress in material science show promise for meeting the accuracy threshold for fault-tolerant quantum computation [118,119]. Whether similar improvement of coherence properties can be achieved for flux qubits remains an open question. Different directions targeting at the experimental implementation of the surface code are actively pursued, either via direct couplings [120] or XcQED layouts [121,122].

The aim of the present work was to contrive a scalable architecture to process quantum information with superconducting qubits. However, we believe that beyond that, ZcQED paves the way for further experimental investigations in quantum optics, thus benefiting from the already existing and vast literature on trapped ions: possible directions include the generation [123–125] and the QND measurement [126–128] of arbitrary quantum states of a quantum harmonic oscillator.

ACKNOWLEDGMENTS

We thank Tsuyoshi Yamamoto for careful reading of our manuscript. P.-M.B. was supported by the RIKEN FPR program. This work was partly funded by ImPACT Program of Council for Science, Technology and Innovation (Cabinet Office, Government of Japan).

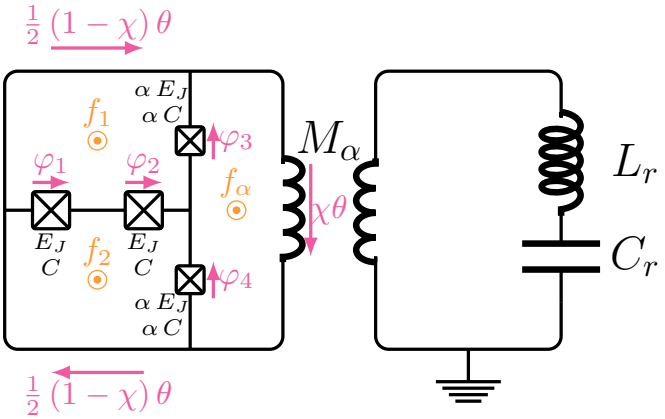

FIG. 14. (Color online) Schematic representation of a tunable gap flux qubit inductively coupled to a quantum harmonic oscillator (lumped element resonator in this case). The interaction with the longitudinal degree of freedom of the artificial atom is achieved by coupling the flux through the split α-junction and the resonator via mutual inductance.

APPENDIX A: FLUX QUBIT LONGITUDINALLY COUPLED TO A RESONATOR

1. Inductive coupling

The most natural way to longitudinally couple a flux qubit to a resonator relies on inductive coupling, as depicted in Fig. 14. As discussed in the foregoing sections, both longitudinal and transverse degrees of freedom of such an artificial atom can be controlled independently and tuned *in situ*. The gap of a flux qubit can be adjusted by splitting the α-junction into two junctions in parallel, thus defining a SQUID whose flux can be tuned in order to control its effective Josephson energy and, in so doing, its gap [129]. The purpose of the gradiometric design represented in Fig. 14 is to access both transverse and longitudinal degrees of freedom separately.

We assume that the self-inductances of loops 1 and 2 are equal, and their area as well. We denote by χ the ratio of the length of the outer part of the α-loop to the total perimeter of the flux trapping loop. The flux quantization conditions for the flux trapping loop, loop 1, loop 2, and the α-loop read respectively as

$$\begin{aligned} \theta + 2\pi\,(f_1 + f_2 + f_\alpha) &= 2\pi\, N \\ \tfrac{1}{2}(1-\chi)\,\theta - \varphi_3 - \varphi_2 - \varphi_1 + 2\pi\, f_1 &= 2\pi\, N_1 \\ \varphi_1 + \varphi_2 - \varphi_4 + \tfrac{1}{2}(1-\chi)\,\theta + 2\pi\, f_2 &= 2\pi\, N_2 \\ \varphi_3 + \chi\,\theta + \varphi_4 + 2\pi\, f_\alpha &= 2\pi\, N_\alpha, \end{aligned} \tag{A1}$$

where φ_i is the phase difference across each junction of the qubit [see Fig. 14]. On the assumption that there is no fluxon trapped in the α-loop ($N_\alpha = 0$), the above conditions can be recast as

$$\begin{aligned} \varphi_3 &= -(\varphi_1 + \varphi_2) - \pi(n - f_\varepsilon) - \pi\,[\chi\,(N - f_\Sigma) + f_\alpha] \\ \varphi_4 &= (\varphi_1 + \varphi_2) + \pi(n - f_\varepsilon) - \pi\,[\chi\,(N - f_\Sigma) + f_\alpha], \end{aligned} \tag{A2}$$

where $N = (N_1 + N_2), n = (N_1 - N_2), f_\Sigma = (f_1 + f_2 + f_\alpha)$, and $f_\varepsilon = (f_1 - f_2)$.

The Lagrangian of the qubit $\mathcal{L}_q$ is found to be

$$\begin{aligned}\mathcal{L}_q &= \mathcal{T} - \mathcal{V} \\ &= (1+2\alpha)\,\frac{C}{2}\,\dot{\phi}_1^2 + 2\alpha\, C\,\dot{\phi}_1\,\dot{\phi}_2 + (1+2\alpha)\,\frac{C}{2}\,\dot{\phi}_2^2 \\ &\quad - E_J(2(1+\alpha) - \cos\varphi_1 - \cos\varphi_2 \\ &\quad - 2\alpha\cos\{\pi[\chi(N-f_\Sigma)+f_\alpha]\} \\ &\quad \times \cos[(\varphi_1+\varphi_2)+\pi(n-f_\varepsilon)]),\end{aligned} \tag{A3}$$

where ϕ_i is the branch flux across each junction of the qubit (i.e., $\phi_i = \Phi_0\,\varphi_i/2\pi$). The charge operators can be obtained by a Legendre transformation of the Lagrangian:

$$\begin{aligned}q_1 &= \frac{\partial\mathcal{L}_q}{\partial\dot{\phi}_1} = (1+2\alpha)\,C\,\dot{\phi}_1 + 2\alpha\,C\,\dot{\phi}_2 \\ q_2 &= \frac{\partial\mathcal{L}_q}{\partial\dot{\phi}_2} = 2\alpha\,C\,\dot{\phi}_1 + (1+2\alpha)\,C\,\dot{\phi}_2.\end{aligned} \tag{A4}$$

We thus deduce that the capacitance matrix is given by

$$\bar{\bar{C}} = \begin{pmatrix}(1+2\alpha)C & 2\alpha\,C \\ 2\alpha\,C & (1+2\alpha)C\end{pmatrix}. \tag{A5}$$

Accordingly, the inverse of the capacitance matrix is found to be

$$\bar{\bar{C}}^{-1} = \frac{1}{(1+4\alpha)\,C}\begin{pmatrix}(1+2\alpha) & -2\alpha \\ -2\alpha & (1+2\alpha)\end{pmatrix}. \tag{A6}$$

Finally, the Hamiltonian of the qubit $\mathcal{H}_q$ reads as

$$\begin{aligned}\mathcal{H}_q &= \frac{1}{2(1+4\alpha)C}\left[(1+2\alpha)q_1^2 - 4\alpha\,q_1\,q_2 + (1+2\alpha)q_2^2\right] \\ &\quad + E_J(2(1+\alpha) - \cos\varphi_1 - \cos\varphi_2 \\ &\quad - 2\alpha\cos\{\pi[\chi(N-f_\Sigma)+f_\alpha]\}, \\ &\quad \times \cos[(\varphi_1+\varphi_2)+\pi(n-f_\varepsilon)]).\end{aligned} \tag{A7}$$

Let us now consider the configuration wherein the current in the resonator is coupled via mutual inductance to the flux through the α-loop of the qubit, as depicted in Fig. 14. Following the Feynman-Hellmann theorem, the transverse and longitudinal coupling constants ($g_\perp$ and $g_\parallel$, respectively) are given by

$$\begin{aligned}g_\perp &= \frac{M_\alpha\,I_r}{\Phi_0}\,\langle 1|\,\frac{\partial\mathcal{H}}{\partial f_\alpha}\,|0\rangle \\ &= 2\pi(1-\chi)\alpha\,E_J\,\frac{M_\alpha\,I_r}{\Phi_0}\,\langle 1|\sin\{\pi[\chi(N-f_\Sigma)+f_\alpha]\} \\ &\quad \times \cos[(\varphi_1+\varphi_2)+\pi(n-f_\varepsilon)]|0\rangle, \\ g_\parallel &= \frac{M_\alpha\,I_r}{\Phi_0}\,\langle +|\frac{\partial\mathcal{H}}{\partial f_\alpha}|-\rangle \\ &= 2\pi(1-\chi)\alpha\,E_J\,\frac{M_\alpha\,I_r}{\Phi_0}\langle +|\sin\{\pi[\chi(N-f_\Sigma)+f_\alpha]\} \\ &\quad \times \cos[(\varphi_1+\varphi_2)+\pi(n-f_\varepsilon)]|-\rangle,\end{aligned} \tag{A8}$$

where $|\pm\rangle = (|0\rangle \pm |1\rangle)/\sqrt{2}$ and $I_r = \sqrt{\omega_r/(2\,L_r)}$ is the current in the resonator.

We ascertain that the transverse coupling $g_\perp$ is zero based on numerical diagonalizations, ergo the Hamiltonian that describes this system is given by

$$\mathcal{H} = \omega_r\,a^\dagger a + \frac{\Delta}{2}\,\sigma_z + g_\parallel\,\sigma_z(a^\dagger + a), \tag{A9}$$

where $\omega_r = \hbar/\sqrt{L_r\,C_r}$ is the resonant frequency of the resonator. We perform numerical calculations to assess the tunability of the gap of the qubit Δ [see Figs. 15(b) and 15(c)], and we also evaluate the longitudinal coupling $g_\parallel$ [see Fig. 15(d)]. Overall, the coupling $g_\parallel$ is proportional to the product of the dependence of the gap as a function of the effective $\alpha_{\rm eff}$, and the variation of $\alpha_{\rm eff}$ as a function of the magnetic flux piercing the α-loop $f_\alpha(g_\parallel \propto \partial\Delta/\partial\alpha_{\rm eff} \times \partial\alpha_{\rm eff}/\partial f_\alpha)$. The achievable longitudinal coupling $g_\parallel$ is a trade-off between the maximum feasible mutual coupling M_α and the sensitivity of the device to the flux noise in the α-loop (qubit dephasing).

2. Capacitive coupling

The possibility of tuning the gap of a flux qubit (rf-SQUID) with a gate voltage via the Aharonov-Casher effect [130,131] was predicted by Friedman and Averin [132]. Their idea was to split the Josephson junction of a rf-SQUID into two junctions of equal Josephson energy in series, and to control the electrostatic potential of the island thus defined. In the single-junction case, the gap of the flux qubit is determined by the fluxon tunneling rate across the junction, which allows one to lift the degeneracy between different persistent current states when the system is biased at half-flux quantum ($\Phi = \Phi_0/2$). In the two-junction case, the gate control allows one to tune the interference between fluxon tunneling across each junction and, accordingly, the gap. A similar idea can be applied to the case of the three-junction flux qubit by splitting the α-junction into two junctions in series. This configuration allows one to simultaneously tune the gap of the qubit via gate control, and to couple other devices to its longitudinal degree of freedom by capacitive coupling. In the following, we will describe how this idea can be applied to the realization of a qubit coupled longitudinally to a quantum harmonic oscillator. The circuit we are considering is depicted in Fig. 16. The Lagrangian $\mathcal{L}$ of this circuit depends on four node fluxes [133,134]: three relating to the artificial atom (ϕ_1, ϕ_2, and ϕ_I) and one relating to the resonator ϕ_r. It is given by

$$\begin{aligned}\mathcal{L} &= \mathcal{T} - \mathcal{V} \\ &= (1+\alpha)\frac{C}{2}\left(\dot{\phi}_1^2 + \dot{\phi}_2^2\right) - \alpha\,C(\dot{\phi}_1+\dot{\phi}_2)\dot{\phi}_I \\ &\quad + \left(\alpha\,C + \frac{C_c}{2} + \frac{C_g}{2}\right)\dot{\phi}_I^2 - C_c\,\dot{\phi}_I\,\dot{\phi}_r + \frac{C_r}{2}\,\dot{\phi}_r^2 \\ &\quad - C_g\,V_g\,\dot{\phi}_I + \frac{C_g}{2}\,V_g^2 \\ &\quad - E_J[2(1+\alpha) - \cos\varphi_1 - \alpha\cos(\varphi_I - \varphi_1) \\ &\quad - \alpha\cos(\varphi_2 - \varphi_I + 2\pi\,f) - \cos\varphi_2] - \frac{\phi_r^2}{2\,L_r},\end{aligned} \tag{A10}$$

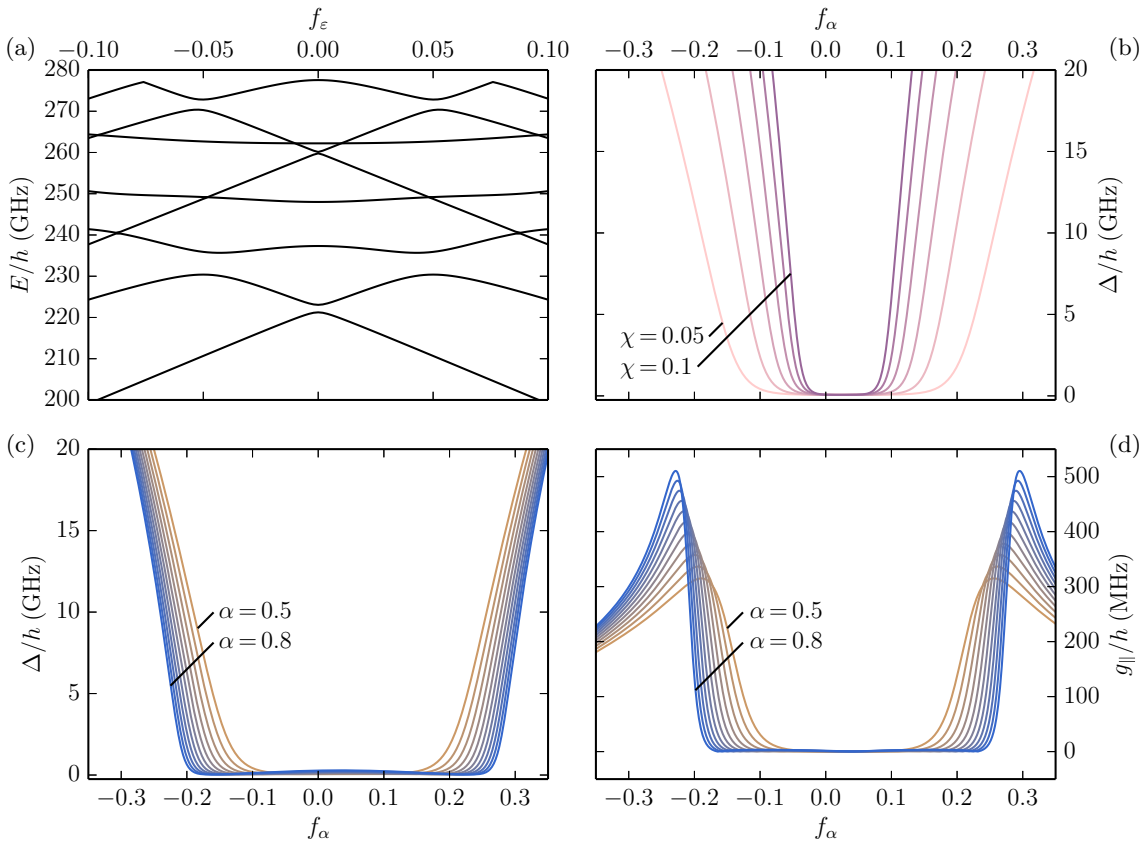

FIG. 15. (Color online) (a) Energy levels of a gradiometric flux qubit as a function of the magnetic frustration $f_\varepsilon(\alpha = 0.5, \chi = 0.05$, and $f_\alpha = 0.2)$. (b) Dependence of the gap Δ on the magnetic flux threading the α-loop f_α for different values of $\chi(\alpha = 0.5)$. Dependence of (c) the gap Δ and (d) the longitudinal coupling $g_\parallel$ on f_α for different values of $\alpha(\chi = 0.05)$. Other parameters are as follows: $C = 8$ fF, $E_J/h = 121$ GHz, $C_r = 250$ fF, $L_r = 1$ nH, and $M_\alpha = 50$ pH. We assume that there is one fluxon trapped in the flux trapping loop $(N = n = 1)$, and that the ratio of the total qubit loop area to the α-loop area $\mathcal{A}_\Sigma/\mathcal{A}_\alpha$ is taken as being equal to 50. These results are obtained by numerical diagonalization of the circuit Hamiltonian with $n_{\rm ch} = 15$ charge states.

where φ_i is the phase corresponding to the node flux ϕ_i (i.e., $\varphi_i = 2\pi\,\phi_i/\Phi_0$), $f = \Phi/\Phi_0$ is the magnetic frustration of the qubit loop, C_g is the gate capacitance, and V_g is the gate voltage applied to tune the electrostatic potential of the island defined by the split α-junction (not represented in Fig. 16). The conjugate momenta of the node fluxes are found by a Legendre transformation of the Lagrangian $\mathcal{L}$:

$$\begin{aligned} q_1 &= \frac{\partial \mathcal{L}}{\partial \dot{\phi}_1}(1+\alpha)C\,\dot{\phi}_1 - \alpha\,C\,\dot{\phi}_I \\ q_2 &= \frac{\partial \mathcal{L}}{\partial \dot{\phi}_2}(1+\alpha)C\,\dot{\phi}_2 - \alpha\,C\,\dot{\phi}_I \\ q_I &= \frac{\partial \mathcal{L}}{\partial \dot{\phi}_I} - \alpha\,C\,\dot{\phi}_1 - \alpha\,C\,\dot{\phi}_2 + (2\,\alpha\,C + C_c)\,\dot{\phi}_I - C_c\,\dot{\phi}_r \\ q_r &= \frac{\partial \mathcal{L}}{\partial \dot{\phi}_r} - C_c\,\dot{\phi}_I + (C_r + C_c)\,\dot{\phi}_r, \end{aligned} \tag{A11}$$

where we assume that $C_g \ll C, C_c$, and $q_I = 2e(n_I + n_g)[n_I$ is the number of excess Cooper pairs on the island delimited by the split α-junction and $n_g = C_g\,V_g/(2e)$ is the reduced gate charge]. The node charges and the time derivative of the node fluxes are linked by the capacitance matrix $(\mathbf{q} = \bar{\bar{C}}\,\dot{\boldsymbol{\phi}})$, which is defined by

$$\bar{\bar{C}} = \begin{pmatrix} (1+\alpha)C & 0 & -\alpha\,C & 0 \\ 0 & (1+\alpha)C & -\alpha\,C & 0 \\ -\alpha\,C & -\alpha\,C & (2\,\alpha\,C + C_c) & -C_c \\ 0 & 0 & -C_c & (C_r + C_c) \end{pmatrix}. \tag{A12}$$

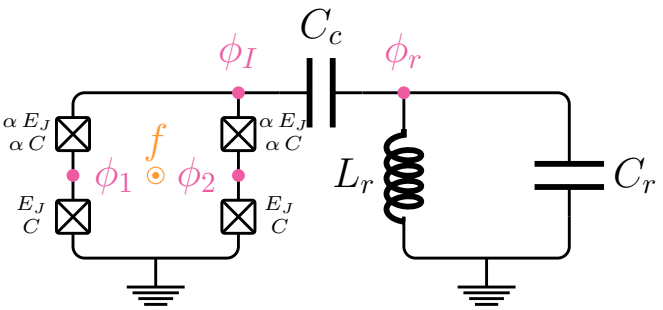

FIG. 16. (Color online) Schematic representation of a tunable gap flux qubit capacitively coupled to a quantum harmonic oscillator: the interaction to the longitudinal degree of freedom of the artificial atom is achieved by coupling the electric potentials of the island defined by the split α-junction and the resonator via a capacitance.

The inverse of the capacitance matrix reads

$$\bar{\bar{C}}^{-1} = \frac{1}{C_0^2}\begin{pmatrix} \alpha\,(2+\alpha)\,C_\Sigma + (1+\alpha)C_\star & \alpha^2\,C_\Sigma & \alpha(1+\alpha)C_\Sigma & \alpha(1+\alpha)C_c \\ \alpha^2\,C_\Sigma & \alpha\,(2+\alpha)\,C_\Sigma + (1+\alpha)C_\star & \alpha(1+\alpha)C_\Sigma & \alpha(1+\alpha)C_c \\ \alpha(1+\alpha)C_\Sigma & \alpha(1+\alpha)C_\Sigma & (1+\alpha)^2 C_\Sigma & (1+\alpha)^2 C_c \\ \alpha(1+\alpha)C_c & \alpha(1+\alpha)C_c & (1+\alpha)^2 C_c & (1+\alpha)\,[2\,\alpha\,C + (1+\alpha)C_c] \end{pmatrix}, \tag{A13}$$

where $C_\Sigma = (C_r + C_c)$, $C_\star = (C_r\,C_c)/C$, and C_0 is defined by $C_0^2 = (1+\alpha)\,[2\,\alpha\,C\,(C_r + C_c) + (1+\alpha)C_r\,C_c]$. Eventually, the Hamiltonian of the circuit is found to be

$$\begin{aligned} \mathcal{H} = {} & \frac{1}{2\,C_0^2}\left[\alpha\,(2+\alpha)\,(C_r + C_c) + (1+\alpha)\frac{C_r\,C_c}{C}\right]\left(q_1^2 + q_2^2\right) + \alpha^2\,\frac{(C_r + C_c)}{C_0^2}\,q_1\,q_2 \\ & + \alpha(1+\alpha)\frac{(C_r + C_c)}{C_0^2}\,(q_1 + q_2)\,q_I + (1+\alpha)^2\frac{(C_r + C_c)}{2\,C_0^2}\,q_I^2 \\ & + \alpha(1+\alpha)\frac{C_c}{C_0^2}\,(q_1 + q_2)\,q_r + (1+\alpha)^2\frac{C_c}{C_0^2}\,q_I\,q_r + (1+\alpha)\frac{2\,\alpha\,C + (1+\alpha)C_c}{2\,C_0^2}\,q_r^2 \\ & + E_J\,[2(1+\alpha) - \cos\varphi_1 - \alpha\cos(\varphi_I - \varphi_1) - \alpha\cos(\varphi_2 - \varphi_I + 2\pi\,f) - \cos\varphi_2] + \frac{\phi_r^2}{2\,L_r}. \end{aligned} \tag{A14}$$

Based on this expression, one can define the transverse and longitudinal coupling constants ($g_\perp$ and $g_\parallel$, respectively) as

$$\begin{aligned} g_\perp &= \langle 1|\sqrt{\frac{\hbar}{2\,Z_r'}}\left[\alpha(1+\alpha)\frac{C_c}{C_0^2}\,(q_1 + q_2) + (1+\alpha)^2\frac{C_c}{C_0^2}\,q_I\right]|0\rangle\,, \\ g_\parallel &= \langle +|\sqrt{\frac{\hbar}{2\,Z_r'}}\left[\alpha(1+\alpha)\frac{C_c}{C_0^2}\,(q_1 + q_2) + (1+\alpha)^2\frac{C_c}{C_0^2}\,q_I\right]|-\rangle\,, \end{aligned} \tag{A15}$$

where $|\pm\rangle = (|0\rangle \pm |1\rangle)/\sqrt{2}$, and $Z_r' = \sqrt{L_r/C_r'}$. The resonator capacitance C_r' renormalized by the interaction with the flux qubit is given by

$$C_r' = \frac{2\,\alpha\,C\,(C_r + C_c) + (1+\alpha)C_r\,C_c}{2\,\alpha\,C + (1+\alpha)C_c}. \tag{A16}$$

We check numerically that the transverse coupling $g_\perp$ is zero. It turns out that the presently considered circuit reduces to a qubit coupled purely via its longitudinal degree of freedom to a quantum harmonic oscillator:

$$\mathcal{H} = \omega_r'\,a^\dagger a + \frac{\Delta}{2}\,\sigma_z + \mathrm{i}\,g_\parallel\,\sigma_z(a^\dagger - a), \tag{A17}$$

where $\omega_r' = \hbar/\sqrt{L_r\,C_r'}$ is the resonant frequency of the resonator. We perform numerical calculations to illustrate the tunability of the gap of the qubit based on the Aharanov-Casher effect [see Figs. 17(a) and 17(b)], and estimate the coupling strengths which can be achieved with some typical parameters [see Figs. 17(c) and 17(d)]. As expected, the longitudinal coupling $g_\parallel$ is maximal when the derivative of the gap versus the gate voltage $\partial\Delta/\partial n_g$ is also maximal, i.e., for $n_g = 0.5$ (mod 1). We note that the longitudinal coupling $g_\parallel$ is saturated when the value of the coupling capacitance C_c is increased, which is a consequence of the renormalization of the effective charging energy of the flux qubit by the interaction with the resonator due to the inversion of the capacitance matrix.

APPENDIX B: DIAGONALIZATION OF TWO QUBITS COUPLED VIA TWO RESONATORS IN Z*p(qq)p*Z CONFIGURATION

The coupling terms between a qubit and a resonator and between both resonators can be equivalently diagonalized in one order or another. Nevertheless, it is preferable to diagonalize the coupling term between resonators first, as this will simplify the treatment of the qubit under the microwave drive. In the first step, we will diagonalize the secular term related to the fixed coupling between both resonators by applying the following unitary transformation:

$$\mathcal{U}_1 = \exp[\theta_1(a^\dagger b - a b^\dagger)]. \tag{B1}$$

The cancellation condition for the secular term reads

$$\tan(2\theta_1) = -\frac{2\,g_c}{\omega_1 - \omega_2}. \tag{B2}$$

In a second step, the nonsecular term can be diagonalized by applying the unitary transformation as follows:

$$\mathcal{U}_2 = \exp[\theta_2(a^\dagger b^\dagger - a b)]. \tag{B3}$$

The cancellation condition for the nonsecular term is given by

$$\tanh(2\theta_2) = \frac{2\cos(2\theta_1)\,g_c}{\omega_1 + \omega_2}. \tag{B4}$$

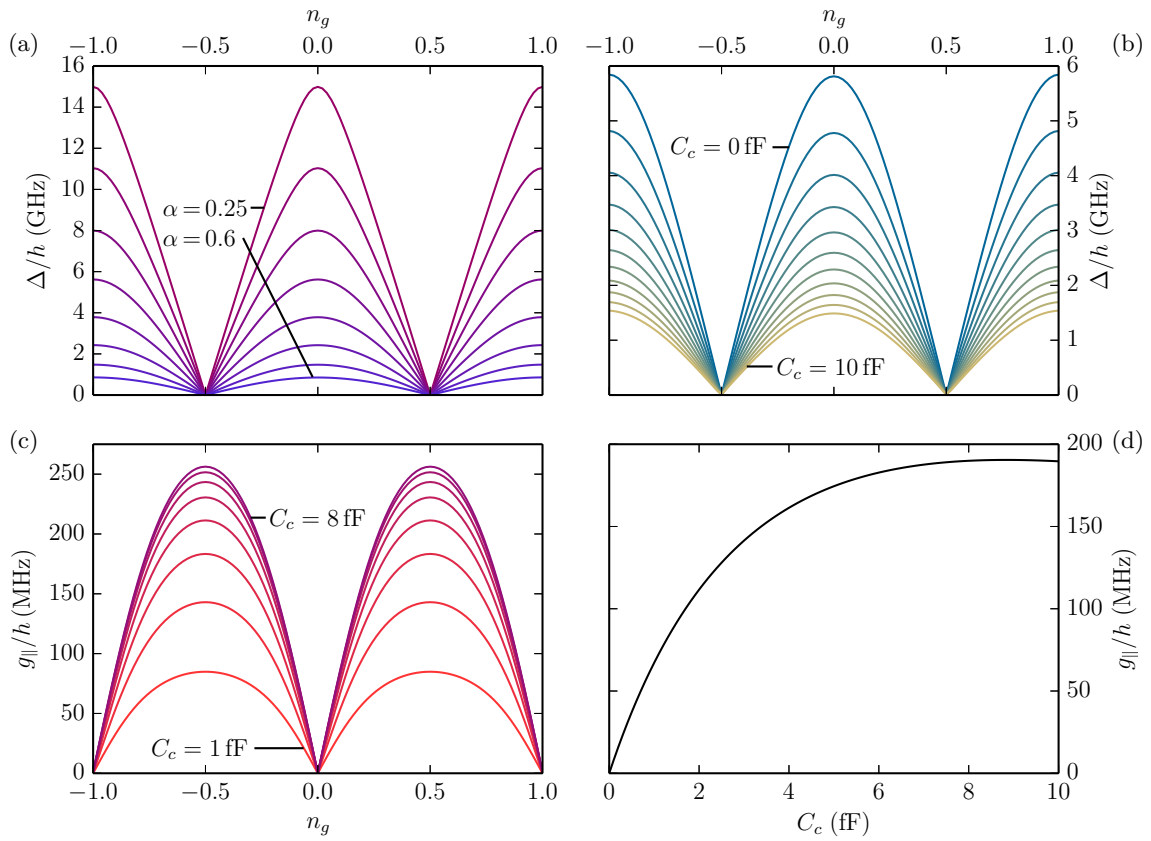

FIG. 17. (Color online) Tunability of the gap vs the reduced gate charge n_g of the island defined by the split α-junction (a) for different values of $\alpha(C_c = 0$ fF) and (b) for different values of the coupling capacitance $C_c(\alpha = 0.4)$. (c) Dependence of the longitudinal coupling $g_\parallel$ on n_g for different values of the coupling capacitance $C_c(\alpha = 0.4)$. (d) Longitudinal coupling $g_\parallel$ as a function of the coupling capacitance $C_c(\alpha = 0.4$ and $n_g = 0.25)$. Other parameters are as follows: $C = 8$ fF, $E_J/h = 121$ GHz, $C_r = 100$ fF, and $L_r = 10$ nH. These results are obtained by numerical diagonalization of the circuit Hamiltonian with $n_{\rm ch} = 7$ charge states.

After diagonalizing the fixed interaction between both resonators, the Hamiltonian is found to be

$$\begin{aligned}\mathcal{H}' = &\overbrace{\left[\cosh(2\theta_2)\frac{\omega_1+\omega_2}{2} - \cos(2\theta_1)\sinh(2\theta_2)g_c\right]}^{\Omega_+}(a^\dagger a + b^\dagger b) + \overbrace{\left[\cos(2\theta_1)\frac{\omega_1-\omega_2}{2} - \sin(2\theta_1)g_c\right]}^{\Omega_-}(a^\dagger a - b^\dagger b)\\ &- \frac{\sin(2\theta_1)}{2}\,g_c[-(a^{\dagger 2}+a^2)+(b^{\dagger 2}+b^2)] + \sum_{i=1,2}\frac{\Delta_i}{2}\,\sigma_i^z\\ &+(\cos\theta_1\cosh\theta_2+\sin\theta_1\sinh\theta_2)g_1\,\sigma_1^z(a^\dagger+a)+(\sin\theta_1\cosh\theta_2+\cos\theta_1\sinh\theta_2)g_1\,\sigma_1^z(b^\dagger+b)\\ &+(-\sin\theta_1\cosh\theta_2+\cos\theta_1\sinh\theta_2)g_2\,\sigma_2^z(a^\dagger+a)+(\cos\theta_1\cosh\theta_2-\sin\theta_1\sinh\theta_2)g_2\,\sigma_2^z(b^\dagger+b).\end{aligned} \tag{B5}$$

In a third step, we diagonalize the two-photon terms associated with each resonator:

$$\mathcal{U}_3 = \exp[\theta_3(a^{\dagger 2}-a^2)+\theta_4(b^{\dagger 2}-b^2)]. \tag{B6}$$

The cancellation conditions for the two-photon terms are found to be

$$\tanh(4\theta_3) = -\frac{\sin(2\theta_1)\,g_c}{\Omega_+ + \Omega_-}, \quad \tanh(4\theta_4) = \frac{\sin(2\theta_1)\,g_c}{\Omega_+ - \Omega_-}. \tag{B7}$$

After diagonalizing the fixed coupling between both resonators, the Hamiltonian reads

$$\begin{aligned}\mathcal{H}'' = &\,\omega_+\,a^\dagger a + \omega_-\,b^\dagger b + \sum_{i=1,2}\frac{\Delta_i}{2}\,\sigma_i^z + (\cos\theta_1\cosh\theta_2+\sin\theta_1\sinh\theta_2)e^{2\theta_3}\,g_1\,\sigma_1^z(a^\dagger+a)\\ &+(\sin\theta_1\cosh\theta_2+\cos\theta_1\sinh\theta_2)e^{2\theta_4}\,g_1\,\sigma_1^z(b^\dagger+b)+(-\sin\theta_1\cosh\theta_2+\cos\theta_1\sinh\theta_2)e^{2\theta_3}\,g_2\,\sigma_2^z(a^\dagger+a)\\ &+(\cos\theta_1\cosh\theta_2-\sin\theta_1\sinh\theta_2)e^{2\theta_4}\,g_2\,\sigma_2^z(b^\dagger+b),\end{aligned} \tag{B8}$$

where $\omega_\pm$ correspond to the resonant frequencies of two fixedly coupled resonators, given by

$$\omega_\pm^2 = \frac{\omega_1^2 + \omega_2^2}{2} \pm \frac{\varsigma}{2}\sqrt{\left(\omega_1^2 - \omega_2^2\right)^2 + 16\, g_c^2\, \omega_1\, \omega_2}, \tag{B9}$$

where $\varsigma = \mathrm{sign}(\omega_1 - \omega_2)$. In the fourth step, the static interaction between qubit 2 and both resonators can be diagonalized by applying the unitary transformation as shown below:

$$\mathcal{U}_4 = \exp\left[-\theta_5\, \sigma_2^z (a^\dagger - a) - \theta_6\, \sigma_2^z (b^\dagger - b)\right]. \tag{B10}$$

The cancellation conditions for the static interaction between qubit 2 and both resonators are given by

$$\theta_5 = \frac{(\cos\theta_1 \sinh\theta_2 - \sin\theta_1 \cosh\theta_2)\, \mathrm{e}^{2\theta_3}\, g_2}{\omega_+}, \quad \theta_6 = \frac{(\cos\theta_1 \cosh\theta_2 - \sin\theta_1 \sinh\theta_2)\, \mathrm{e}^{2\theta_4}\, g_2}{\omega_-}. \tag{B11}$$

Eventually, the static interaction between qubit 1 and both resonators can be diagonalized by applying the unitary transformation:

$$\mathcal{U}_5 = \exp\left[-\theta_7\, \sigma_1^z (a^\dagger - a) - \theta_8\, \sigma_1^z (b^\dagger - b)\right]. \tag{B12}$$

The cancellation conditions for the static interaction between qubit 1 and both resonators read

$$\theta_7 = \frac{(\cos\theta_1 \cosh\theta_2 + \sin\theta_1 \sinh\theta_2)\, \mathrm{e}^{2\theta_3}\, g_1}{\omega_+}, \quad \theta_8 = \frac{(\cos\theta_1 \sinh\theta_2 + \sin\theta_1 \cosh\theta_2)\, \mathrm{e}^{2\theta_4}\, g_1}{\omega_-}. \tag{B13}$$

[1] A. J. Leggett, Macroscopic quantum systems and the quantum theory of measurement, Prog. Theor. Phys. Suppl. **69**, 80 (1980).

[2] M. H. Devoret, J. M. Martinis, and J. Clarke, Measurements of macroscopic quantum tunneling out of the zero-voltage state of a current-biased Josephson junction, Phys. Rev. Lett. **55**, 1908 (1985).

[3] Y. Nakamura, Yu. A. Pashkin, and J. S. Tsai, Coherent control of macroscopic quantum states in a single-Cooper-pair box, Nature (London) **398**, 786 (1999).

[4] J. E. Mooij, T. P. Orlando, L. Levitov, L. Tian, C. H. van der Wal, and S. Lloyd, Josephson persistent-current qubit, Science **285**, 1036 (1999).

[5] I. Chiorescu, Y. Nakamura, C. J. P. M. Harmans, and J. E. Mooij, Coherent quantum dynamics of a superconducting flux qubit, Science **299**, 1869 (2003).

[6] J. Koch, T. M. Yu, J. Gambetta, A. A. Houck, D. I. Schuster, J. Majer, A. Blais, M. H. Devoret, S. M. Girvin, and R. J. Schoelkopf, Charge-insensitive qubit design derived from the Cooper pair box, Phys. Rev. A **76**, 042319 (2007).

[7] J. A. Schreier, A. A. Houck, J. Koch, D. I. Schuster, B. R. Johnson, J. M. Chow, J. M. Gambetta, J. Majer, L. Frunzio, M. H. Devoret, S. M. Girvin, and R. J. Schoelkopf, Suppressing charge noise decoherence in superconducting charge qubits, Phys. Rev. B **77**, 180502(R) (2008).

[8] A. J. Berkley, H. Xu, R. C. Ramos, M. A. Gubrud, F. W. Strauch, P. R. Johnson, J. R. Anderson, A. J. Dragt, C. J. Lobb, and F. C. Wellstood, Entangled macroscopic quantum states in two superconducting qubits, Science **300**, 1548 (2003).

[9] L. DiCarlo, M. D. Reed, L. Sun, B. R. Johnson, J. M. Chow, J. M. Gambetta, L. Frunzio, S. M. Girvin, M. H. Devoret, and R. J. Schoelkopf, Preparation and measurement of three-qubit entanglement in a superconducting circuit, Nature (London) **467**, 574 (2010).

[10] M. Neeley, R. C. Bialczak, M. Lenander, E. Lucero, M. Mariantoni, A. D. O'Connell, D. Sank, H. Wang, M. Weides, J. Wenner, Y. Yin, T. Yamamoto, A. N. Cleland, and J. M. Martinis, Generation of three-qubit entangled states using superconducting phase qubits, Nature (London) **467**, 570 (2010).

[11] L. DiCarlo, J. M. Chow, J. M. Gambetta, L. S. Bishop, B. R. Johnson, D. I. Schuster, J. Majer, A. Blais, L. Frunzio, S. M. Girvin, and R. J. Schoelkopf, Demonstration of two-qubit algorithms with a superconducting quantum processor, Nature (London) **460**, 240 (2009).

[12] T. Yamamoto, M. Neeley, E. Lucero, R. C. Bialczak, J. Kelly, M. Lenander, M. Mariantoni, A. D. O'Connell, D. Sank, H. Wang, M. Weides, J. Wenner, Y. Yin, A. N. Cleland, and J. M. Martinis, Quantum process tomography of two-qubit controlled-Z and controlled-NOT gates using superconducting phase qubits, Phys. Rev. B **82**, 184515 (2010).

[13] E. Lucero, R. Barends, Y. Chen, J. Kelly, M. Mariantoni, A. Megrant, P. O'Malley, D. Sank, A. Vainsencher, J. Wenner, T. White, Y. Yin, A. N. Cleland, and J. M. Martinis, Computing prime factors with a Josephson phase qubit quantum processor, Nat. Phys. **8**, 719 (2012).

[14] M. D. Reed, L. DiCarlo, S. E. Nigg, L. Sun, L. Frunzio, S. M. Girvin, and R. J. Schoelkopf, Realization of three-qubit quantum error correction with superconducting circuits, Nature (London) **482**, 382 (2012).

[15] D. P. DiVincenzo, The physical implementation of quantum computation, Fortschr. Phys. **48**, 771 (2000).

[16] P. W. Shor, Scheme for reducing decoherence in quantum computer memory, Phys. Rev. A **52**, R2493(R) (1995).

[17] A. Yu. Kitaev, Fault-tolerant quantum computation by anyons, Ann. Phys. **303**, 2 (2003).

[18] S. B. Bravyi and A. Yu. Kitaev, Quantum codes on a lattice with boundary, arXiv:quant-ph/9811052.

[19] M. H. Freedman and D. A. Meyer, Projective plane and planar quantum codes, Found. Comput. Math. **1**, 325 (2001).

[20] R. Raussendorf and J. Harrington, Fault-tolerant quantum computation with high threshold in two dimensions, Phys. Rev. Lett. **98**, 190504 (2007).

[21] A. G. Fowler, A. M. Stephens, and P. Groszkowski, High-threshold universal quantum computation on the surface code, Phys. Rev. A **80**, 052312 (2009).

[22] D. S. Wang, A. G. Fowler, and L. C. L. Hollenberg, Surface code quantum computing with error rates over 1%, Phys. Rev. A **83**, 020302(R) (2011).
[23] A. G. Fowler, M. Mariantoni, J. M. Martinis, and A. N. Cleland, Surface codes: Towards practical large-scale quantum computation, Phys. Rev. A **86**, 032324 (2012).
[24] J.-M. Raimond, M. Brune, and S. Haroche, Manipulating quantum entanglement with atoms and photons in a cavity, Rev. Mod. Phys. **73**, 565 (2001).
[25] S. Haroche and J.-M. Raimond, *Exploring the Quantum: Atoms, Cavities, and Photons* (Oxford University Press, Oxford, 2006).
[26] E. Hagley, X. Maître, G. Nogues, C. Wunderlich, M. Brune, J.-M. Raimond, and S. Haroche, Generation of Einstein-Podolsky-Rosen pairs of atoms, Phys. Rev. Lett. **79**, 1 (1997).
[27] A. Rauschenbeutel, G. Nogues, S. Osnaghi, P. Bertet, M. Brune, J.-M. Raimond, and S. Haroche, Coherent operation of a tunable quantum phase gate in cavity QED, Phys. Rev. Lett. **83**, 5166 (1999).
[28] X. Maître, E. Hagley, G. Nogues, C. Wunderlich, P. Goy, M. Brune, J.-M. Raimond, and S. Haroche, Quantum memory with a single photon in a cavity, Phys. Rev. Lett. **79**, 769 (1997).
[29] D. Leibfried, R. Blatt, C. Monroe, and D. J. Wineland, Quantum dynamics of single trapped ions, Rev. Mod. Phys. **75**, 281 (2003).
[30] Q. A. Turchette, C. S. Wood, B. E. King, C. J. Myatt, D. Leibfried, W. M. Itano, C. Monroe, and D. J. Wineland, Deterministic entanglement of two trapped ions, Phys. Rev. Lett. **81**, 3631 (1998).
[31] C. A. Sackett, D. Kielpinski, B. E. King, C. Langer, V. Meyer, C. J. Myatt, M. Rowe, Q. A. Turchette, W. M. Itano, D. J. Wineland, and C. Monroe, Experimental entanglement of four particles, Nature (London) **404**, 256 (2000).
[32] T. Monz, P. Schindler, J. T. Barreiro, M. Chwalla, D. Nigg, W. A. Coish, M. Harlander, W. Hänsel, M. Hennrich, and R. Blatt, 14-Qubit entanglement: Creation and coherence, Phys. Rev. Lett. **106**, 130506 (2011).
[33] S. Gulde, M. Riebe, G. P. T. Lancaster, C. Becher, J. Eschner, H. Häffner, F. Schmidt-Kaler, I. L. Chuang, and R. Blatt, Implementation of the Deutsch-Jozsa algorithm on an ion-trap quantum computer, Nature (London) **421**, 48 (2003).
[34] T. Monz, K. Kim, W. Hänsel, M. Riebe, A. S. Villar, P. Schindler, M. Chwalla, M. Hennrich, and R. Blatt, Realization of the quantum Toffoli gate with trapped ions, Phys. Rev. Lett. **102**, 040501 (2009).
[35] J. Chiaverini, D. Leibfried, T. Schaetz, M. D. Barrett, R. B. Blakestad, J. Britton, W. M. Itano, J. D. Jost, E. Knill, C. Langer, R. Ozeri, and D. J. Wineland, Realization of quantum error correction, Nature (London) **432**, 602 (2004).
[36] P. Schindler, J. T. Barreiro, T. Monz, V. Nebendahl, D. Nigg, M. Chwalla, M. Hennrich, and R. Blatt, Experimental repetitive quantum error correction, Science **332**, 1059 (2011).
[37] J. I. Cirac and P. Zoller, Quantum computations with cold trapped ions, Phys. Rev. Lett. **74**, 4091 (1995).
[38] C. Monroe, D. M. Meekhof, B. E. King, W. M. Itano, and D. J. Wineland, Demonstration of a fundamental quantum logic gate, Phys. Rev. Lett. **75**, 4714 (1995).
[39] F. Schmidt-Kaler, H. Häffner, M. Riebe, S. Gulde, G. P. T. Lancaster, T. Deuschle, C. Becher, C. F. Roos, J. Eschner, and R. Blatt, Realization of the Cirac-Zoller controlled-NOT quantum gate, Nature (London) **422**, 408 (2003).
[40] J. I. Cirac and P. Zoller, A scalable quantum computer with ions in an array of microtraps, Nature (London) **404**, 579 (2000).
[41] D. Kielpinski, C. Monroe, and D. J. Wineland, Architecture for a large-scale ion-trap quantum computer, Nature (London) **417**, 709 (2002).
[42] A. Blais, R.-S. Huang, A. Wallraff, S. M. Girvin, and R. J. Schoelkopf, Cavity quantum electrodynamics for superconducting electrical circuits: An architecture for quantum computation, Phys. Rev. A **69**, 062320 (2004).
[43] A. Wallraff, D. I. Schuster, A. Blais, L. Frunzio, R.-S. Huang, J. Majer, S. Kumar, S. M. Girvin, and R. J. Schoelkopf, Strong coupling of a single photon to a superconducting qubit using circuit quantum electrodynamics, Nature (London) **431**, 162 (2004).
[44] T. P. Orlando, J. E. Mooij, L. Tian, C. H. van der Wal, L. S. Levitov, S. Lloyd, and J. J. Mazo, Superconducting persistent-current qubit, Phys. Rev. B **60**, 15398 (1999).
[45] H. Paik, D. I. Schuster, L. S. Bishop, G. Kirchmair, G. Catelani, A. P. Sears, B. R. Johnson, M. J. Reagor, L. Frunzio, L. I. Glazman, S. M. Girvin, M. H. Devoret, and R. J. Schoelkopf, Observation of high coherence in Josephson junction qubits measured in a three-dimensional circuit QED architecture, Phys. Rev. Lett. **107**, 240501 (2011).
[46] E. T. Jaynes and F. W. Cummings, Comparison of quantum and semiclassical radiation theories with application to the beam maser, Proc. IEEE **51**, 89 (1963).
[47] A. Wallraff, D. I. Schuster, A. Blais, L. Frunzio, J. Majer, M. H. Devoret, S. M. Girvin, and R. J. Schoelkopf, Approaching unit visibility for control of a superconducting qubit with dispersive readout, Phys. Rev. Lett. **95**, 060501 (2005).
[48] E. M. Purcell, Spontaneous emission probabilities at radio frequencies, Phys. Rev. **69**, 681 (1946).
[49] A. A. Houck, J. A. Schreier, B. R. Johnson, J. M. Chow, J. Koch, J. M. Gambetta, D. I. Schuster, L. Frunzio, M. H. Devoret, S. M. Girvin, and R. J. Schoelkopf, Controlling the spontaneous emission of a superconducting transmon qubit, Phys. Rev. Lett. **101**, 080502 (2008).
[50] I. I. Rabi, Space quantization in a gyrating magnetic field, Phys. Rev. **51**, 652 (1937).
[51] D. Braak, Integrability of the Rabi model, Phys. Rev. Lett. **107**, 100401 (2011).
[52] D. Zueco, G. M. Reuther, S. Kohler, and P. Hänggi, Qubit-oscillator dynamics in the dispersive regime: Analytical theory beyond the rotating-wave approximation, Phys. Rev. A **80**, 033846 (2009).
[53] A. Blais, J. Gambetta, A. Wallraff, D. I. Schuster, S. M. Girvin, M. H. Devoret, and R. J. Schoelkopf, Quantum-information processing with circuit quantum electrodynamics, Phys. Rev. A **75**, 032329 (2007).
[54] A. Wallraff, D. I. Schuster, A. Blais, J. M. Gambetta, J. Schreier, L. Frunzio, M. H. Devoret, S. M. Girvin, and R. J. Schoelkopf, Sideband transitions and two-tone spectroscopy of a superconducting qubit strongly coupled to an on-chip cavity, Phys. Rev. Lett. **99**, 050501 (2007).
[55] P. J. Leek, S. Filipp, P. Maurer, M. Baur, R. Bianchetti, J. M. Fink, M. Göppl, L. Steffen, and A. Wallraff, Using sideband transitions for two-qubit operations in superconducting circuits, Phys. Rev. B **79**, 180511(R) (2009).

[56] P. J. Leek, M. Baur, J. M. Fink, R. Bianchetti, L. Steffen, S. Filipp, and A. Wallraff, Cavity quantum electrodynamics with separate photon storage and qubit readout modes, Phys. Rev. Lett. **104**, 100504 (2010).

[57] F. Beaudoin, M. P. da Silva, Z. Dutton, and A. Blais, First-order sidebands in circuit QED using qubit frequency modulation, Phys. Rev. A **86**, 022305 (2012).

[58] J. D. Strand, M. Ware, F. Beaudoin, T. A. Ohki, B. R. Johnson, A. Blais, and B. L. T. Plourde, First-order sideband transitions with flux-driven asymmetric transmon qubits, Phys. Rev. B **87**, 220505(R) (2013).

[59] See Supplemental Material at http://link.aps.org/supplemental/10.1103/PhysRevB.91.094517 for certain calculation details, intermediary approaches and animations showing the time-evolution of the photon number distribution in the readout resonator.

[60] M. A. Sillanpää, J. I. Park, and R. W. Simmonds, Coherent quantum state storage and transfer between two phase qubits via a resonant cavity, Nature (London) **449**, 438 (2007).

[61] J. Majer, J. M. Chow, J. M. Gambetta, J. Koch, B. R. Johnson, J. A. Schreier, L. Frunzio, D. I. Schuster, A. A. Houck, A. Wallraff, A. Blais, M. H. Devoret, S. M. Girvin, and R. J. Schoelkopf, Coupling superconducting qubits via a cavity bus, Nature (London) **449**, 443 (2007).

[62] F. W. Strauch, P. R. Johnson, A. J. Dragt, C. J. Lobb, J. R. Anderson, and F. C. Wellstood, Quantum logic gates for coupled superconducting phase qubits, Phys. Rev. Lett. **91**, 167005 (2003).

[63] C. Rigetti and M. Devoret, Fully microwave-tunable universal gates in superconducting qubits with linear couplings and fixed transition frequencies, Phys. Rev. B **81**, 134507 (2010).

[64] J. M. Chow, A. D. Córcoles, J. M. Gambetta, C. Rigetti, B. R. Johnson, J. A. Smolin, J. R. Rozen, G. A. Keefe, M. B. Rothwell, M. B. Ketchen, and M. Steffen, Simple all-microwave entangling gate for fixed-frequency superconducting qubits, Phys. Rev. Lett. **107**, 080502 (2011).

[65] J. M. Chow, J. M. Gambetta, A. W. Cross, S. T. Merkel, C. Rigetti, and M. Steffen, Microwave-activated conditional-phase gate for superconducting qubits, New J. Phys. **15**, 115012 (2013).

[66] S. Poletto, J. M. Gambetta, S. T. Merkel, J. A. Smolin, J. M. Chow, A. D. Córcoles, G. A. Keefe, M. B. Rothwell, J. R. Rozen, D. W. Abraham, C. Rigetti, and M. Steffen, Entanglement of two superconducting qubits in a waveguide cavity via monochromatic two-photon excitation, Phys. Rev. Lett. **109**, 240505 (2012).

[67] F. Helmer, M. Mariantoni, A. G. Fowler, J. von Delft, E. Solano, and F. Marquardt, Cavity grid for scalable quantum computation with superconducting circuits, Europhys. Lett. **85**, 50007 (2009).

[68] A. Galiautdinov, A. N. Korotkov, and J. M. Martinis, Resonator-zero-qubit architecture for superconducting qubits, Phys. Rev. A **85**, 042321 (2012).

[69] J. Ghosh, A. Galiautdinov, Z. Zhou, A. N. Korotkov, J. M. Martinis, and M. R. Geller, High-fidelity controlled-σ^z gate for resonator-based superconducting quantum computers, Phys. Rev. A **87**, 022309 (2013).

[70] M. Mariantoni, H. Wang, T. Yamamoto, M. Neeley, R. C. Bialczak, Y. Chen, M. Lenander, E. Lucero, A. D. O'Connell, D. Sank, M. Weides, J. Wenner, Y. Yin, J. Zhao, A. N. Korotkov, A. N. Cleland, and J. M. Martinis, Implementing the quantum von Neumann architecture with superconducting circuits, Science **334**, 61 (2011).

[71] P. Bertet, C. J. P. M. Harmans, and J. E. Mooij, Parametric coupling for superconducting qubits, Phys. Rev. B **73**, 064512 (2006).

[72] A. O. Niskanen, Y. Nakamura, and J. S. Tsai, Tunable coupling scheme for flux qubits at the optimal point, Phys. Rev. B **73**, 094506 (2006).

[73] D. J. Wineland and W. M. Itano, Laser cooling of atoms, Phys. Rev. A **20**, 1521 (1979).

[74] W. Vogel and R. L. de Matos Filho, Nonlinear Jaynes-Cummings dynamics of a trapped ion, Phys. Rev. A **52**, 4214 (1995).

[75] R. H. Dicke, The effect of collisions upon the Doppler width of spectral lines, Phys. Rev. **89**, 472 (1953).

[76] Y.-D. Wang, A. Kemp, and K. Semba, Coupling superconducting flux qubits at optimal point via dynamic decoupling with the quantum bus, Phys. Rev. B **79**, 024502 (2009).

[77] A. J. Kerman, Quantum information processing using quasiclassical electromagnetic interactions between qubits and electrical resonators, New J. Phys. **15**, 123011 (2013).

[78] K. Mølmer and A. Sørensen, Multiparticle entanglement of hot trapped ions, Phys. Rev. Lett. **82**, 1835 (1999).

[79] A. Sørensen and K. Mølmer, Quantum computation with ions in thermal motion, Phys. Rev. Lett. **82**, 1971 (1999).

[80] A. Sørensen and K. Mølmer, Entanglement and quantum computation with ions in thermal motion, Phys. Rev. A **62**, 022311 (2000).

[81] D. Leibfried, B. DeMarco, V. Meyer, D. Lucas, M. Barrett, J. Britton, W. M. Itano, B. Jelenković, C. Langer, T. Rosenband, and D. J. Wineland, Experimental demonstration of a robust, high-fidelity geometric two ion-qubit phase gate, Nature (London) **422**, 412 (2003).

[82] P. C. Haljan, K.-A. Brickman, L. Deslauriers, P. J. Lee, and C. Monroe, Spin-dependent forces on trapped ions for phase-stable quantum gates and entangled states of spin and motion, Phys. Rev. Lett. **94**, 153602 (2005).

[83] J. Benhelm, G. Kirchmair, C. F. Roos, and R. Blatt, Towards fault-tolerant quantum computing with trapped ions, Nat. Phys. **4**, 463 (2008).

[84] I. G. Lang and Yu. A. Firsov, Kinetic theory of semiconductors with low mobility, Sov. Phys. JETP **16**, 1301 (1963).

[85] B. E. King, C. S. Wood, C. J. Myatt, Q. A. Turchette, D. Leibfried, W. M. Itano, C. Monroe, and D. J. Wineland, Cooling the collective motion of trapped ions to initialize a quantum register, Phys. Rev. Lett. **81**, 1525 (1998).

[86] J. M. Fink, M. Göppl, M. Baur, R. Bianchetti, P. J. Leek, A. Blais, and A. Wallraff, Climbing the Jaynes-Cummings ladder and observing its nonlinearity in a cavity QED system, Nature (London) **454**, 315 (2008).

[87] D. Leibfried, D. M. Meekhof, B. E. King, C. Monroe, W. M. Itano, and D. J. Wineland, Experimental determination of the motional quantum state of a trapped atom, Phys. Rev. Lett. **77**, 4281 (1996).

[88] D. M. Meekhof, C. Monroe, B. E. King, W. M. Itano, and D. J. Wineland, Generation of nonclassical motional states of a trapped atom, Phys. Rev. Lett. **76**, 1796 (1996).

[89] M. Boissonneault, J. M. Gambetta, and A. Blais, Dispersive regime of circuit QED: Photon-dependent qubit dephasing and relaxation rates, Phys. Rev. A **79**, 013819 (2009).
[90] D. Kleppner, Inhibited spontaneous emission, Phys. Rev. Lett. **47**, 233 (1981).
[91] G. Gabrielse and H. Dehmelt, Observation of inhibited spontaneous emission, Phys. Rev. Lett. **55**, 67 (1985).
[92] P. Goy, J.-M. Raimond, M. Gross, and S. Haroche, Observation of cavity-enhanced single-atom spontaneous emission, Phys. Rev. Lett. **50**, 1903 (1983).
[93] R. G. Hulet, E. S. Hilfer, and D. Kleppner, Inhibited spontaneous emission by a Rydberg atom, Phys. Rev. Lett. **55**, 2137 (1985).
[94] G. S. Solomon, M. Pelton, and Y. Yamamoto, Single-mode spontaneous emission from a single quantum dot in a three-dimensional microcavity, Phys. Rev. Lett. **86**, 3903 (2001).
[95] M. D. Reed, B. R. Johnson, A. A. Houck, L. DiCarlo, J. M. Chow, D. I. Schuster, L. Frunzio, and R. J. Schoelkopf, Fast reset and suppressing spontaneous emission of a superconducting qubit, Appl. Phys. Lett. **96**, 203110 (2010).
[96] J. M. Gambetta, A. A. Houck, and A. Blais, Superconducting qubit with Purcell protection and tunable coupling, Phys. Rev. Lett. **106**, 030502 (2011).
[97] A. Steane, C. F. Roos, D. Stevens, A. Mundt, D. Leibfried, F. Schmidt-Kaler, and R. Blatt, Speed of ion-trap quantum-information processors, Phys. Rev. A **62**, 042305 (2000).
[98] H. Häffner, S. Gulde, M. Riebe, G. Lancaster, C. Becher, J. Eschner, F. Schmidt-Kaler, and R. Blatt, Precision measurement and compensation of optical Stark shifts for an ion-trap quantum processor, Phys. Rev. Lett. **90**, 143602 (2003).
[99] C. Monroe, D. Leibfried, B. E. King, D. M. Meekhof, W. M. Itano, and D. J. Wineland, Simplified quantum logic with trapped ions, Phys. Rev. A **55**, R2489(R) (1997).
[100] A. M. Childs and I. L. Chuang, Universal quantum computation with two-level trapped ions, Phys. Rev. A **63**, 012306 (2000).
[101] H. G. Dehmelt, Proposed $10^{14}\,\Delta\nu < \nu$ laser fluorescence spectroscopy on Ti^{+} mono-ion oscillator II, Bull. Am. Phys. Soc. **20**, 60 (1975).
[102] W. Nagourney, J. Sandberg, and H. Dehmelt, Shelved optical electron amplifier: Observation of quantum jumps, Phys. Rev. Lett. **56**, 2797 (1986).
[103] Th. Sauter, W. Neuhauser, R. Blatt, and P. E. Toschek, Observation of quantum jumps, Phys. Rev. Lett. **57**, 1696 (1986).
[104] J. C. Bergquist, R. G. Hulet, W. M. Itano, and D. J. Wineland, Observation of quantum jumps in a single atom, Phys. Rev. Lett. **57**, 1699 (1986).
[105] A. H. Myerson, D. J. Szwer, S. C. Webster, D. T. C. Allcock, M. J. Curtis, G. Imreh, J. A. Sherman, D. N. Stacey, A. M. Steane, and D. M. Lucas, High-fidelity readout of trapped-ion qubits, Phys. Rev. Lett. **100**, 200502 (2008).
[106] B. G. U. Englert, G. Mangano, M. Mariantoni, R. Gross, J. Siewert, and E. Solano, Mesoscopic shelving readout of superconducting qubits in circuit quantum electrodynamics, Phys. Rev. B **81**, 134514 (2010).
[107] Y. Yin, Y. Chen, D. Sank, P. J. J. O'Malley, T. C. White, R. Barends, J. Kelly, E. Lucero, M. Mariantoni, A. Megrant, C. Neill, A. Vainsencher, J. Wenner, A. N. Korotkov, A. N. Cleland, and J. M. Martinis, Catch and release of microwave photon states, Phys. Rev. Lett. **110**, 107001 (2013).
[108] R. C. Bialczak, M. Ansmann, M. Hofheinz, M. Lenander, E. Lucero, M. Neeley, A. D. O'Connell, D. Sank, H. Wang, M. Weides, J. Wenner, T. Yamamoto, A. N. Cleland, and J. M. Martinis, Fast tunable coupler for superconducting qubits, Phys. Rev. Lett. **106**, 060501 (2011).
[109] D. I. Schuster, A. Wallraff, A. Blais, L. Frunzio, R.-S. Huang, J. Majer, S. M. Girvin, and R. J. Schoelkopf, ac Stark shift and dephasing of a superconducting qubit strongly coupled to a cavity field, Phys. Rev. Lett. **94**, 123602 (2005).
[110] J. Gambetta, A. Blais, D. I. Schuster, A. Wallraff, L. Frunzio, J. Majer, M. H. Devoret, S. M. Girvin, and R. J. Schoelkopf, Qubit-photon interactions in a cavity: Measurement-induced dephasing and number splitting, Phys. Rev. A **74**, 042318 (2006).
[111] H. Y. Carr and E. M. Purcell, Effects of diffusion on free precession in nuclear magnetic resonance experiments, Phys. Rev. **94**, 630 (1954).
[112] S. Meiboom and D. Gill, Modified spin-echo method for measuring nuclear relaxation times, Rev. Sci. Instrum. **29**, 688 (1958).
[113] L. Viola and S. Lloyd, Dynamical suppression of decoherence in two-state quantum systems, Phys. Rev. A **58**, 2733 (1998).
[114] L. Viola, E. Knill, and S. Lloyd, Dynamical decoupling of open quantum systems, Phys. Rev. Lett. **82**, 2417 (1999).
[115] P. Zanardi, Symmetrizing evolutions, Phys. Lett. A **258**, 77 (1999).
[116] G. S. Uhrig, Keeping a quantum bit alive by optimized π-pulse sequences, Phys. Rev. Lett. **98**, 100504 (2007).
[117] J. Bylander, S. Gustavsson, F. Yan, F. Yoshihara, K. Harrabi, G. Fitch, D. G. Cory, Y. Nakamura, J. S. Tsai, and W. D. Oliver, Noise spectroscopy through dynamical decoupling with a superconducting flux qubit, Nat. Phys. **7**, 565 (2011).
[118] R. Barends, J. Kelly, A. Megrant, D. Sank, E. Jeffrey, Y. Chen, Y. Yin, B. Chiaro, J. Mutus, C. Neill, P. O'Malley, P. Roushan, J. Wenner, T. C. White, A. N. Cleland, and J. M. Martinis, Coherent Josephson qubit suitable for scalable quantum integrated circuits, Phys. Rev. Lett. **111**, 080502 (2013).
[119] J. B. Chang, M. R. Vissers, A. D. Córcoles, M. Sandberg, J. Gao, D. W. Abraham, J. M. Chow, J. M. Gambetta, M. B. Rothwell, G. A. Keefe, M. Steffen, and D. P. Pappas, Improved superconducting qubit coherence using titanium nitride, Appl. Phys. Lett. **103**, 012602 (2013).
[120] R. Barends, J. Kelly, A. Megrant, A. Veitia, D. Sank, E. Jeffrey, T. C. White, J. Mutus, A. G. Fowler, B. Campbell, Y. Chen, Z. Chen, B. Chiaro, A. Dunsworth, C. Neill, P. O'Malley, P. Roushan, A. Vainsencher, J. Wenner, A. N. Korotkov, A. N. Cleland, and J. M. Martinis, Superconducting quantum circuits at the surface code threshold for fault tolerance, Nature (London) **508**, 500 (2014).
[121] D. P. DiVincenzo, Fault-tolerant architectures for superconducting qubits, Phys. Scr. **T137**, 014020 (2009).
[122] J. M. Chow, J. M. Gambetta, E. Magesan, D. W. Abraham, A. W. Cross, B. R. Johnson, N. A. Masluk, C. A. Ryan, J. A. Smolin, S. J. Srinivasan, and M. Steffen, Implementing a strand of a scalable fault-tolerant quantum computing fabric, Nat. Commun. **5**, 4015 (2014).

[123] B. Kneer and C. K. Law, Preparation of arbitrary entangled quantum states of a trapped ion, Phys. Rev. A **57**, 2096 (1998).

[124] G. Drobný, B. Hladký, and V. Bužek, Quantum-state synthesis of multimode bosonic fields: Preparation of arbitrary states of two-dimensional vibrational motion of trapped ions, Phys. Rev. A **58**, 2481 (1998).

[125] A. Ben-Kish, B. DeMarco, V. Meyer, M. Rowe, J. Britton, W. M. Itano, B. M. Jelenković, C. Langer, D. Leibfried, T. Rosenband, and D. J. Wineland, Experimental demonstration of a technique to generate arbitrary quantum superposition states of a harmonically bound spin-1/2 particle, Phys. Rev. Lett. **90**, 037902 (2003).

[126] C. D'Helon and G. J. Milburn, Measuring the vibrational energy of a trapped ion, Phys. Rev. A **52**, 4755 (1995).

[127] R. L. de Matos Filho and W. Vogel, Quantum nondemolition measurement of the motional energy of a trapped atom, Phys. Rev. Lett. **76**, 4520 (1996).

[128] L. Davidovich, M. Orszag, and N. Zagury, Quantum nondemolition measurements of vibrational populations in ionic traps, Phys. Rev. A **54**, 5118 (1996).

[129] F. G. Paauw, A. Fedorov, C. J. P. M. Harmans, and J. E. Mooij, Tuning the gap of a superconducting flux qubit, Phys. Rev. Lett. **102**, 090501 (2009).

[130] Y. Aharonov and A. Casher, Topological quantum effects for neutral particles, Phys. Rev. Lett. **53**, 319 (1984).

[131] B. Reznik and Y. Aharonov, Question of the nonlocality of the Aharonov-Casher effect, Phys. Rev. D **40**, 4178 (1989).

[132] J. R. Friedman and D. V. Averin, Aharonov-Casher-effect suppression of macroscopic tunneling of magnetic flux, Phys. Rev. Lett. **88**, 050403 (2002).

[133] B. Yurke and J. S. Denker, Quantum network theory, Phys. Rev. A **29**, 1419 (1984).

[134] M. H. Devoret, Quantum Fluctuations in Electrical Circuits, in *Quantum Fluctuations*, Les Houches, Session LXIII, 1995, edited by S. Reynaud, E. Giacobino, and J. Zinn-Justin (Elsevier, Amsterdam, 1997), pp. 351–386.